Article

Cell Chemical Biology

Leveraging Compound Promiscuity to Identify Targetable Cysteines within the Kinome

Graphical Abstract

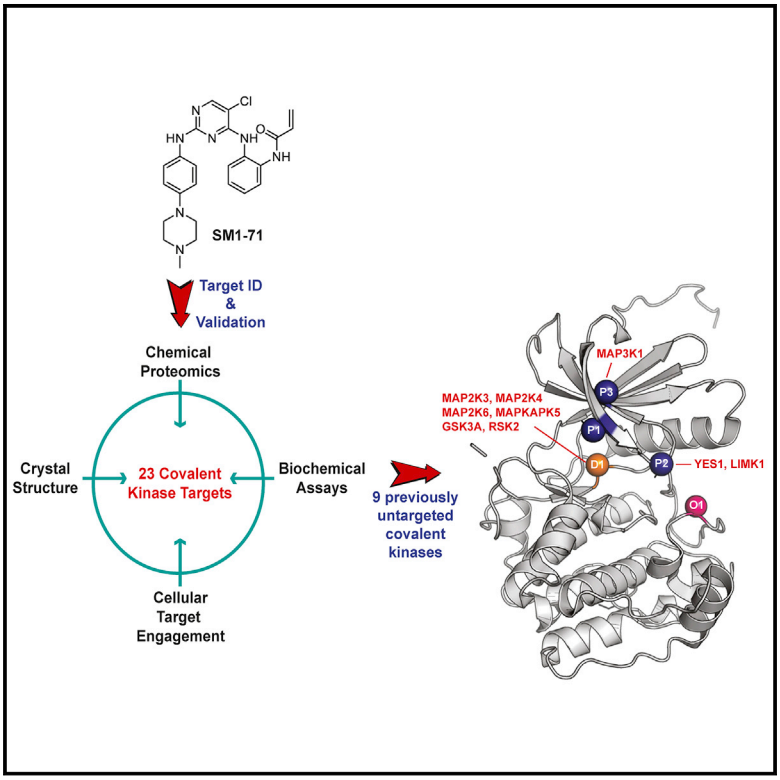

Authors

Suman Rao, Deepak Gurbani, Guangyan Du, ..., Kenneth D. Westover, Peter K. Sorger, Nathanael S. Gray

Correspondence

peter_sorger@hms.harvard.edu (P.K.S.), nathanael_gray@dfci.harvard.edu (N.S.G.)

In Brief

The current work by Rao et al. describes using a promiscuous ligand as a tool to identify new targets for drug discovery. The findings from this study highlight previously unknown targets against which irreversible inhibitors can be developed. These targets are typically deregulated in diseases including cancer.

Highlights

- Our study highlights a multi-targeted strategy to identify druggable cysteines
- We identified 23 covalent kinase targets across multiple spatial locations
- Nine of these have previously not been covalently targeted by an inhibitor
- Our findings highlight potential means to advance covalent drug discovery efforts

Rao et al., 2019, Cell Chemical Biology *26*, 818–829
June 20, 2019
https://doi.org/10.1016/j.chembiol.2019.02.021

CellPress

CellPress

Cell Chemical Biology
Article

Leveraging Compound Promiscuity to Identify Targetable Cysteines within the Kinome

Suman Rao,[1,2,3] Deepak Gurbani,[4] Guangyan Du,[2,3] Robert A. Everley,[1] Christopher M. Browne,[2,3,5] Apirat Chaikuad,[6,7] Li Tan,[2,3] Martin Schröder,[6,7] Sudershan Gondi,[4] Scott B. Ficarro,[2,3,5] Taebo Sim,[8,9] Nam Doo Kim,[10] Matthew J. Berberich,[1] Stefan Knapp,[6,7,11] Jarrod A. Marto,[2,3,5] Kenneth D. Westover,[4] Peter K. Sorger,[1,*] and Nathanael S. Gray[2,3,12,*]

[1]Laboratory of Systems Pharmacology, Harvard Medical School, Boston, MA 02115, USA
[2]Department of Cancer Biology, Dana-Farber Cancer Institute, Boston, MA 02115, USA
[3]Department of Biological Chemistry and Molecular Pharmacology, Harvard Medical School, Boston, MA 02115, USA
[4]Departments of Biochemistry and Radiation Oncology, The University of Texas Southwestern Medical Center at Dallas, Dallas, TX 75390, USA
[5]Blais Proteomics Center, Dana-Farber Cancer Institute, Boston, MA 02115, USA
[6]Institute of Pharmaceutical Chemistry, Goethe-University Frankfurt, Max von Lauestr. 9, 60438 Frankfurt am Main, Germany
[7]Buchmann Institute for Life Sciences (BMLS) and Structural Genomics Consortium Goethe-University Frankfurt, Max von Lauestr. 9, 60438 Frankfurt am Main, Germany
[8]Chemical Kinomics Research Center, Korea Institute of Science and Technology (KIST), 5 Hwarangro 14-gil, Seongbuk-gu, Seoul 02792, Republic of Korea
[9]KU-KIST Graduate School of Converging Science and Technology, Korea University, 145 Anam-ro, Seongbuk-gu, Seoul 02841, Republic of Korea
[10]NDBio Therapeutics Inc., Incheon 21984, Republic of Korea
[11]German Cancer Network (DKTK), Frankfurt Site, 60438 Frankfurt am Main, Germany
[12]Lead Contact
*Correspondence: peter_sorger@hms.harvard.edu (P.K.S.), nathanael_gray@dfci.harvard.edu (N.S.G.)
https://doi.org/10.1016/j.chembiol.2019.02.021

SUMMARY

Covalent kinase inhibitors, which typically target cysteine residues, represent an important class of clinically relevant compounds. Approximately 215 kinases are known to have potentially targetable cysteines distributed across 18 spatially distinct locations proximal to the ATP-binding pocket. However, only 40 kinases have been covalently targeted, with certain cysteine sites being the primary focus. To address this disparity, we have developed a strategy that combines the use of a multi-targeted acrylamide-modified inhibitor, SM1-71, with a suite of complementary chemoproteomic and cellular approaches to identify additional targetable cysteines. Using this single multi-targeted compound, we successfully identified 23 kinases that are amenable to covalent inhibition including MKNK2, MAP2K1/2/3/4/6/7, GAK, AAK1, BMP2K, MAP3K7, MAPKAPK5, GSK3A/B, MAPK1/3, SRC, YES1, FGFR1, ZAK (MLTK), MAP3K1, LIMK1, and RSK2. The identification of nine of these kinases previously not targeted by a covalent inhibitor increases the number of targetable kinases and highlights opportunities for covalent kinase inhibitor development.

INTRODUCTION

Kinases play an important role in regulating cellular functions such as proliferation, survival, death, invasion, metabolism, and differentiation. Deregulation of kinase activity leads to aberrant cellular signaling resulting in diverse pathological conditions including oncogenic transformation. In the last two decades, 31 kinase inhibitors have been approved for the treatment of a variety of cancers (Zhang et al., 2017). The majority of these drugs are reversible ATP-competitive inhibitors that bind to kinases in a "DFG-in" or "DFG-out" conformation (Wu et al., 2016), while only five are covalent kinase inhibitors. In general, covalent inhibitors are designed to contain an electrophilic warhead (e.g., acrylamide or vinyl sulfonates) and bind target proteins in a two-step process involving non-covalent recognition and binding, followed by covalent bond formation with an accessible nucleophile, usually a cysteine. In kinases, the positions of the cysteine and warhead must be compatible for a covalent bond to form (Liu et al., 2013; Singh et al., 2011).

Covalent kinase inhibitors present several potential advantages over their reversible counterparts including (1) improved selectivity over other targets due to binding of non-conserved cysteine residues, (2) stronger potency owing to high-affinity binding between drug and target, (3) beneficial pharmacodynamics from irreversible target binding leading to prolonged target inhibition, and (4) overcoming resistance to reversible kinase inhibitors that can no longer inhibit kinases due to acquired mutations in the binding site (Singh et al., 2011). Targetable cysteines on kinases are spatially distributed and can be classified into different groups based on their accessibility and position. Previously, Liu et al. (2013) identified 18 spatial cysteine positions using an informatics study based on primary sequence alignment of kinases that belonged to the gatekeeper, DFG, glycine-rich, hinge, and roof regions. Among these, only a handful of kinases belonging to the DFG–1, glycine-rich loop and hinge regions were covalently targeted by inhibitors (Liu et al., 2013). Another study by Zhao et al. (2017b) used function-site

interaction fingerprint and density functional theory calculations across 2,774 kinase-ligand complex structures and mapped out 17 cysteine locations within the active site. The authors further noted that of all the covalent kinase inhibitors designed to date, 62% targeted cysteines in the front pocket (e.g., EGFR, BTK, or JAK3), 26% targeted the P-loop region (e.g., FGFR1-4), and <10% targeted other positions (Zhao et al., 2017b). It is thus not surprising that the only five approved covalent kinase inhibitors (afatinib, osimertinib, dacomitinib, ibrutinib, and neratinib) target kinases with cysteines in the front pocket (i.e., EGFR, BTK, and HER2) (Dungo and Keating, 2013; Chakraborty et al., 2015; Davids and Brown, 2014; Cameron and Sanford, 2014; Greig, 2016; Deeks, 2017; Shirley, 2018; Cancer Discovery, 2017). These studies highlight the fact that, despite the existence of ~215 kinases with accessible cysteines within the kinome, only 40 have been experimentally demonstrated to be covalently targeted. In addition, despite 18 spatially distinct cysteine positions available, only a subset (~10) have been explored for covalent modification (Chaikuad et al., 2018).

Together, this motivated us to explore additional cysteines that could be targeted by a small-molecule covalent kinase inhibitor. Recently, we utilized a strategy involving a multi-targeted degrader to scan the proteome for easily degradable kinases (Huang et al., 2018). In our current study, we implement a conceptually similar strategy by employing a multi-targeted ligand, SM1-71, to identify covalently targetable kinases within the proteome. Using complementary chemoproteomic, biochemical, and cellular assays, we discovered that SM1-71 covalently inhibits 23 kinases with cysteines located in the DFG–1, P-loop, and activation loop regions of the kinase domain. We further identified that, among these, nine kinases have previously never been covalently targeted by an inhibitor (not including covalent fragments such as iodoacetamide probes). These findings significantly increase the number of kinases that can be covalently targeted and expand the sites at which cysteines can be covalently modified.

RESULTS

Preliminary Mapping of Kinases Amenable to Irreversible Inhibition Using the Multi-targeted Compound, SM1-71

Our primary goal was to use SM1-71 as a multi-targeted compound to scan the proteome for covalently modified kinases (Figure S1; Data S1). This compound was chosen from a small library of previously synthesized covalent kinase inhibitors with a 2,4-disubstituted pyrimidine scaffold, designed to target the DFG–1 cysteine on TAK1 (Tan et al., 2017a). SM1-71 contains an acrylamide warhead in the *ortho*-position and exhibited off-target binding toward kinases other than TAK1 with a DFG–1 cysteine (Tan et al., 2017a), suggesting that it might serve as a multi-targeted probe to interrogate the cellular kinome. Given that the 2,4-diaminopyrimidine scaffold is a well-explored pharmacophore capable of binding potently to nucleotide-binding pockets in both a covalent and non-covalent fashion, we first developed SM1-71-R, a reversible analog of SM1-71 to use as a control compound to distinguish between covalent and non-covalent modes of action (Figure S1; Data S1). To examine the target space of SM1-71, we used multiplexed inhibitor beads (MIBs) (Duncan et al., 2012), also known as kinobeads (Bantscheff et al., 2007; Lemeer et al., 2013; Médard et al., 2015). MIBs consist of multiple kinase inhibitor scaffolds bound covalently to beads that serve as an affinity matrix for diverse kinases. In the presence of a competing small-molecule inhibitor, binding to the beads is reduced, and this reduction can be quantified by mass spectrometry (MS) analysis. We performed our cell-based assays primarily in the H23-KRAS^{G12C} non-small-cell lung cancer (NSCLC) cell line, which is potently inhibited by SM1-71 (half maximal inhibitory concentration [IC_{50}] = 0.4 μM) as seen in proliferation assays (Figure S2A). We chose this cell line for its sensitivity toward SM1-71 in an anti-proliferative screen, when compared with multiple other cancer cell lines (Rao et al., 2019). To distinguish covalent from reversibly bound targets, we monitored the kinetics of target engagement by SM1-71 in a "washout assay" and included SM1-71-R as a control compound. In brief, H23-KRAS^{G12C} NSCLC cells, which are potently inhibited by SM1-71 (IC_{50} = 0.4 μM) as seen in proliferation assays (Figure S2A), were incubated with 1 μM SM1-71 or SM1-71-R or DMSO for 4 h followed by media exchange to wash out the compound; cells were then harvested 0, 2, 4, 6, and 24 h post washout. Cell lysates were incubated with MIBs to recover kinases that were not stably (and presumably, covalently) bound to the compound. MIB-associated proteins were eluted, digested and labeled with isobaric tags (e.g., tandem mass tag). Samples were then subjected to MS analysis and peptide signals corresponding to kinases pulled down by the beads were quantified. We set a 1.5-fold difference in MIB binding for SM1-71 over the DMSO control as the cutoff for differentially bound kinases 0, 2, 4, and 6 h post washout (Data S2A). This generated a list of 54 kinases potentially targeted by SM1-71 described in Table S1.

To better distinguish between those kinases that are inhibited via a covalent mode of inhibition, from those that engage non-covalently, we computed a binding index (BI) that represents the ratio between kinases pulled down by MIBs in extracts from cells treated with SM1-71 and SM1-71-R and then subjected to washout for a period of time (t). We designated kinases with BI $\leq$ 0.5 at t = 0 and 6 h ($BI_{0h,6h}$) after washout as potentially irreversible and those with $BI_{0h,6h}$ > 0.5 as potentially reversible (Table 1). Kinases having $BI_{0h,6h} \leq 0.5$ included GAK, MAP2K1 (MEK1), MAP2K2 (MEK2), MAPK1 (ERK2), and SRC, to name a few (see Table 1 for the full list of kinases), several of which contained a DFG–1 cysteine. The remaining kinases largely demonstrated patterns of reversible inhibition, as indicated by their BI values (>0.5). ACVR1 showed a decrease in its BI value, likely indicating irreversible binding 6 h post washout or a slow off-rate. AURKA, TEC, and PTK2 (FAK) showed $BI_{0h,6h}$ >1, suggesting a strong preference for reversible mode of inhibition. AURKA in particular, showed a BI_{6h} of 2.4, which is indicative of stronger binding by SM1-71-R compared with SM1-71. We suspected that this results from a slow off-rate and confirmed this using the NanoBRET assay in HEK293T cells (Figures S3A–S3C).

Evaluating Kinase Binding Potency Using Cell-Based and Biochemical Assays

We determined binding potency of kinase inhibition in H23 cell lysates using an MIB assay (Data S2B) and corroborated the inhibition of several of these kinases using a biochemical assay

Table 1. List of Kinases Inhibited by SM1-71 in an MIB Assay

Kinase	BI_{0h}	BI_{6h}	Binding
GAK	0.07	0.04	irreversible
MAP2K2	0.03	0.18	irreversible
YES1	0.21	0.1	irreversible
MAP2K1	0.05	0.36	irreversible
AAK1	0.27	0.32	irreversible
SRC	0.19	0.13	irreversible
BMP2K	0.23	0.27	irreversible
LIMK1	0.21	0.23	irreversible
MAP3K1	0.2	0.54	irreversible
MAPK1	0.19	0.39	irreversible
FGFR1	0.45	0.42	irreversible
PIK3C3	0.28	0.44	irreversible
PIK3R4	0.36	0.47	irreversible
CSNK2A1	0.8	0.64	reversible
DDR1	0.68	0.59	reversible
MET	0.75	0.53	reversible
EPHA10	0.72	0.63	reversible
CSNK1E	0.79	0.58	reversible
EPHB2	0.7	0.5	reversible
EPHA2	0.71	0.49	reversible
PIP4K2C	0.8	0.6	reversible
AGK	0.66	0.5	reversible
EIF2AK3	0.8	0.66	reversible
PKMYT1	0.47	0.8	reversible
CDK9	0.46	0.96	reversible
STK16	0.51	0.76	reversible
IGF1R	0.45	0.64	reversible
PIP5K1A	0.56	0.75	reversible
INSR	0.52	0.76	reversible
TGFBR2	0.53	0.6	reversible
CDK13	0.57	0.57	reversible
CSNK1G1	0.55	0.81	reversible
CDK17	0.46	0.76	reversible
PRKD3	0.59	0.72	reversible
MAP3K11	0.6	0.76	reversible
MAPK3	0.62	0.54	reversible
LYN	1.1	0.79	reversible
HCK	1.3	0.85	reversible
TGFBR1	1.09	0.8	reversible
WEE1	0.98	0.63	reversible
ACVR1B	0.9	0.92	reversible
MARK2	0.74	1.13	reversible
TK2	0.83	0.95	reversible
FYN	0.81	0.91	reversible
PRKDC	0.76	0.77	reversible
CSNK1A1	0.91	0.74	reversible
CSNK1D	0.71	0.78	reversible
TNIK	0.67	0.74	reversible
CSNK1G3	0.77	0.75	reversible
PAK4	0.93	0.9	reversible
AURKA	1.16	2.38	strongly reversible
TEC	1.02	1.43	strongly reversible
PTK2	1.3	1.12	strongly reversible
ACVR1	0.81	0.3	weakly irreversible

Note: Kinases showing >1.5-fold inhibition at all time points up to 6 h post washout are represented here.

(Table S2). The biochemical IC_{50} values correlated well with IC_{50} values from the MIB assay, with several kinases displaying comparable values (Table S2). For instance, irreversibly inhibited kinases such as GAK, YES1, AAK1, SRC, LIMK1, MAP2K1, and MAP2K2, and reversibly inhibited kinases such as PTK2, AURKA, IGF1R, and TGFBR2, showed good agreement between the two assays. However, there were instances in which IC_{50} values diverged between MIB and biochemical assays; for example, MAPK1, MAPK3, TEC, and MET (Table S2). The reasons for these differences are not known but might reflect different states of covalent modification or a different spectrum of binding partners. We further compared the kinase inhibitory potency of SM1-71 and SM1-71-R in the biochemical assay. Our results showed that SM1-71-R was a weaker inhibitor of kinases that previously demonstrated irreversible inhibition by SM1-71. For instance, kinases such as GAK, MAP2K1, MAP2K2, MAPK1, LIMK1, and SRC showed 6- to 67-fold stronger inhibition by SM1-71 than SM1-71-R. Similarly, reversibly bound kinases such as AURKA, PTK2 (FAK), TEC, IGF1R, and MET showed equivalent inhibition by both SM1-71 and SM1-71-R (Table S2). These results suggest that the electrophilic warhead of SM1-71 enables it to potently bind targets in both a covalent and non-covalent manner.

Our results suggest that SM1-71 is able to potently engage several kinase targets through both reversible and irreversible binding; many irreversibly bound kinases lack the DFG–1 cysteine, suggesting that SM1-71 might be interacting with cysteines located in other positions. We therefore performed additional chemoproteomic analysis to annotate potential cysteines labeled and validate covalent targets of SM1-71.

Site-Level Proteomic Identification of Cysteines Modified by SM1-71

To complement the MIB approach, we employed a direct affinity capture strategy to identify specific cysteine sites modified by SM1-71 using a qualitative cysteine-labeling technique (Ficarro et al., 2016). To facilitate enrichment of labeled peptides from complex cellular lysates, we synthesized a desthiobiotin (DTB)-tagged analog of SM1-71 (SM1-71-DTB) that enables efficient capture on streptavidin-coated beads (Figure S4A). To increase the coverage of kinases we performed the assay using two KRAS mutant NSCLC cells lines, H23-$KRAS^{G12C}$ and Calu-6-$KRAS^{Q61K}$, which showed strong growth inhibitory effects by SM1-71 (Figure S2). We screened cysteines within the kinome amenable to covalent modification, on treatment with a higher dose of SM1-71-DTB. To this end, cell lysates were incubated

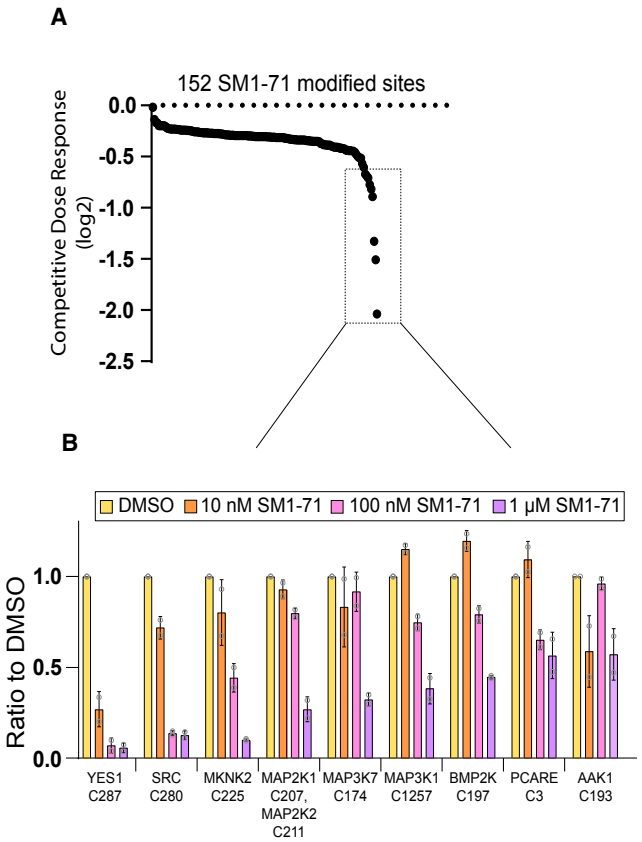

Figure 1. Covalent Inhibitor Target Site Identification (CITe-Id) in H23-KRAS^{G12C} Cells

(A) Cysteine sites modified by SM1-71-DTB in a dose-dependent manner across the whole proteome. Inhibitor concentrations and log2 ratios were used to generate a linear trendline with y-intercept ser at zero for each labeled site. The conpetitive dose-response was the slope of this trendline. All reproducibly detected sites were then rank-ordered. The dased-box shows the sites with a competitive dose-response two standard deviations from the mean.

(B) Bar charts showing individual competition ratios for the nine sites that showed significant dose-dependent labeling by SM1-71-DTB compared with the DMSO-treated samples (>2 SD). Untransformed ratios are shown for clarity. The data represented here are from two independent biological replicates. Bars are the mean of the ratio of a condition from each biological replicate with standard deviation error bars and individual data points as grey circles.

with DMSO or 2 μM SM1-71-DTB overnight followed by trypsin digestion. Peptides covalently bound by SM1-71-DTB were isolated using streptavidin resin and then processed and analyzed by liquid chromatography-tandem MS (Ficarro et al., 2009). As described previously (Ficarro et al., 2016), we modified our data-pipeline to account for fragment ions associated with SM1-71-DTB. Overall, we identified >1,000 cysteine residues that react covalently with SM1-71-DTB in Calu-6 and H23 cells, respectively (Data S2C and S2D). Several non-kinase cysteine residues were labeled with SM1-71-DTB, which is commonly observed in this type of labeling experiment, potentially due to capture of hyper-reactive cysteines in the proteome (Weerapana et al., 2010; Lanning et al., 2014).

We detected 23 gene-unique peptides containing labeled cysteines belonging to 21 kinases, distributed at different spatial locations including the activation loop, DFG–1, DFG+3, hinge, and P-loop regions (Table S7). Eleven of the 23 labeled cysteines were identified in the DFG–1 position, which is the original cysteine position that SM1-71 was designed to inhibit in MAP3K7 (TAK1). The second most prominent location labeled was within the P-loop and included nine kinases (Table S7). We also identified labeling of C225 of MKNK2 in the activation loop, C180 of MAP3K7 in the DFG+3 position, and C172 of PLK4 in the hinge region. In addition to the 23 peptides labeled uniquely from a particular protein, we identified 6 non-unique peptides containing labeled cysteines, each of which mapped to multiple kinases. For example, we identified a peptide containing a labeled cysteine in the DFG–1 position that maps to one or more kinases including MAPK1, FLT4 (VEGFR3), KDR (VEGFR2), FLT3, KIT, NLK, FLT1, PDGFRA, or PDGFRB. Five out of the six non-unique peptides showed cysteine labeling at the DFG–1 position; only one peptide showed cysteine labeling in the activation loop (Table S7).

Next, we sought to identify which of these kinases could be covalently labeled in a competitive dose-dependent manner. To this end, we implemented our recently published methodology termed covalent inhibitor target-site identification (CITe-Id) (Browne et al., 2018), which is a chemoproteomic technique that directly measures and quantifies dose-dependent labeling of cysteines across the proteome. We pretreated H23-KRAS^{G12C} cells with 10, 100, and 1,000 nM of SM1-71 or DMSO for 2 h, followed by drug washout, cell extraction, and lysis. The lysate was then incubated with 2 μM of SM1-71-DTB to competitively bind targets weakly bound or unbound by SM1-71 during cellular pretreatment. Samples were subsequently analyzed and our results showed that 152 cysteine sites were commonly labeled by SM1-71-DTB in the two biological replicates of the experiment (Figure 1A). We identified a total of 15 kinases labeled in this experiment, among which nine kinases showed significant labeling in a dose-dependent manner compared with the DMSO-treated control (>2 SD) (Data S2E; Table S7). YES1 (C287) showed >50% labeling at 10 nM, while SRC (C280) and MKNK2 (C225) showed >50% labeling at 100 nM (Figure 1B). The remaining kinases including MAP2K1 (C207), MAP2K2 (C211), MAP3K1 (C1257), BMP2K (C197), MAP3K7 (C174), and AAK1 (C193) showed >50% labeling at 1 μM concentration (Figure 1B). All of these kinases were detected in the qualitative cysteine-labeling experiment.

Orthogonal Assays to Validate Covalently Labeled Kinases

In our initial cysteine-labeling experiment, we identified 23 kinases with modified cysteines (through gene-unique peptides) and a few additional kinases with non-unique peptides. Fourteen of these kinases were also detected in the MIB assay that showed at least 1.5-fold inhibition 0, 2, 4, and 6 h post washout compared with the DMSO-treated control (Table 1). Furthermore, we noted that seven out of the nine kinases that were labeled in a dose-dependent manner in the CITe-Id experiment were also irreversibly inhibited ($BI_{0h,6h} \leq 0.5$) in the MIB assay (78% overlap). Although there is significant overlap between the two chemoproteomic approaches, there are covalent targets detected in a single assay that require additional validation to confirm or dispute (e.g., PIK3C3, MAP2K7, MAPK3, TNK1). To address this, we performed additional validation

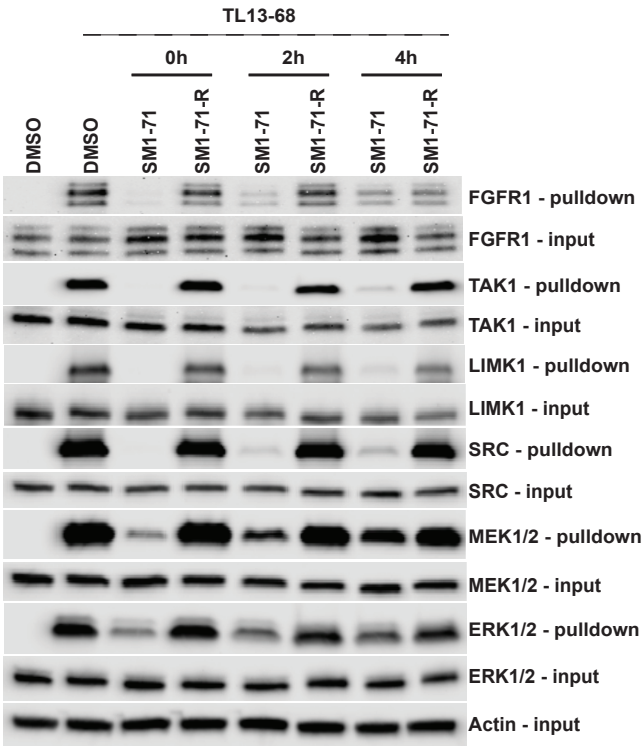

Figure 2. Cellular Target Engagement in H23-KRAS^{G12C} Cells to Confirm Sustained Inhibition of Covalent Targets

H23-KRAS^{G12C} cells were treated with 1 μM of SM1-71 or SM1-71-R or DMSO for 2 h followed by drug washout. Cells were collected and lysed at different intervals post washout and incubated with 1 μM of TL13-68, a biotin-tagged version of SM1-71 that competes for the binding pocket of the target kinase. Kinases previously unbound by SM1-71 or SM1-71-R and bound by TL13-68 were pulled down by streptavidin agarose resin and detected using western blotting. We monitored total levels of kinase present in each of the samples by collecting lysate before pull-down by the beads (indicated by inputs). We probed for FGFR1, TAK1 (MAP3K7), LIMK1, SRC, MEK1/2, and ERK1/2 using antibodies to measure the level of kinase inhibition (indicated by pull-down). The above figure is a representation from one of two independent biological replicates performed.

experiments and classified kinases as covalent targets if they showed irreversible inhibition in at least two orthogonal experiments.

Covalent Adduct Formation

We used a thermal stability shift assay (T_m shift) that exploits the fact that proteins stably bound to chemical ligands often have increased thermal stability. We subsequently used MS to monitor formation of covalent adducts by mass shift (Vedadi et al., 2006). SM1-71 was screened against 43 recombinant kinases using temperature shift (ΔT_m) assays; of these 21 kinases exhibited ΔT_m shifts of >6°C, which is indicative of complex formation (Table S3). We then incubated each of these 21 kinases with SM1-71 for 4 and 24 h, and measured mass shifts using electrospray time-of-flight MS (Table S4). Our results showed that nine kinases formed covalent adducts with SM1-71 including GAK, MAP2K7, GSK3B, MAPK3, SRC, MAP2K1, MAP2K2, MAPK1, and MAP2K6 (Figure 4). All of these kinases overlapped with kinases previously identified in one or more assays (Table S7).

SM1-71-Derivatized Beads Pull-Down

As a complementary means to quantify covalently inhibited kinases we used SM1-71-derivatized agarose beads to pull down enriched kinases (Figure S4B). SM1-71-derivatized beads (N-Hydroxysuccinimidyl-Sepharose) were incubated with H23-KRAS^{G12C} cell lysate pretreated with 1 μM SM1-71 or DMSO, and beads were subjected to stringent washes using SDS-containing buffers to ensure removal of non-covalently bound targets. Kinases demonstrating at least 1.5-fold higher pull-down in the DMSO-treated sample compared with the SM1-71 pretreated sample were judged to be irreversibly bound by SM1-71. This generated a list of 51 kinases (Table S5, Data S2F), among which 19 kinases overlapped with those previously identified in one or more assays (Table S7; Figure 4).

Cellular Target Engagement

We investigated target engagement of a few kinases using a pull-down assay in H23-KRAS^{G12C} cells to further validate covalent labeling by SM1-71. In brief, cells were treated with 1 μM of SM1-71 or SM1-71-R or DMSO for 2 h, followed by drug washout and replacement with fresh drug-free media. Cells were collected and lysed 0, 2, and 4 h post washout, and incubated with 1 μM of a biotin-tagged version of SM1-71, TL13-68 (Figure S4C), that competes to bind kinase targets of SM1-71. Kinases unbound by SM1-71 or SM1-71-R were bound by TL13-68 and pulled down using streptavidin beads and detected using western blotting. We included SM1-71-R as a reversible control compound, which is incapable of forming covalent bonds or inducing sustained target engagement. Our results showed that SRC, LIMK1, FGFR, and TAK1 (MAP3K7) showed strong and sustained inhibition by SM1-71, even 4 h post washout. MEK1/2 and ERK1/2 were inhibited up to 2 h post washout with almost complete loss of inhibition 4 h post washout. As expected, SM1-71-R that lacks a covalent warhead failed to inhibit any of the targets (Figure 2). Together these data confirm irreversible inhibition of eight kinases in cells, all of which overlapped with kinases previously identified in one or more assays (Table S7; Figure 4).

Co-crystal Structures Illustrating Covalent Bond Formation

Chemoproteomics identified several covalent targets of SM1-71 with cysteine residues in different spatial locations (e.g., DFG–1, P-loop). Based on previous work with inhibitors that covalently target both EGFR and FGFR, which possess spatially distinct cysteine residues (Tan et al., 2014), we speculated that the acrylamide "arm" of SM1-71 might use different orientations to reach spatially distinct cysteine residues. In particular, we were interested in elucidating the binding mode between SM1-71 and the P-loop cysteine, which is shared among nine different kinases including SRC, YES1, FGR, TNK1, LIMK1, FGFR1, FGFR2, FGFR3, and FGFR4. To determine how this occurs we used X-ray crystallography to solve crystal structures of SRC bound to SM1-71 (PDB: 6ATE). In addition, we also solved the crystal structures of ERK1 (PDB: 6GES) and ERK2 (PDB: 6G54) bound to SM1-71 to illustrate the binding mode with a DFG–1 cysteine. These crystal structures and their comparison with a published structure of SM1-71 with TAK1 (Tan et al., 2017a) offered an opportunity to visualize different binding poses of SM1-71 and rationalize the observed promiscuity.

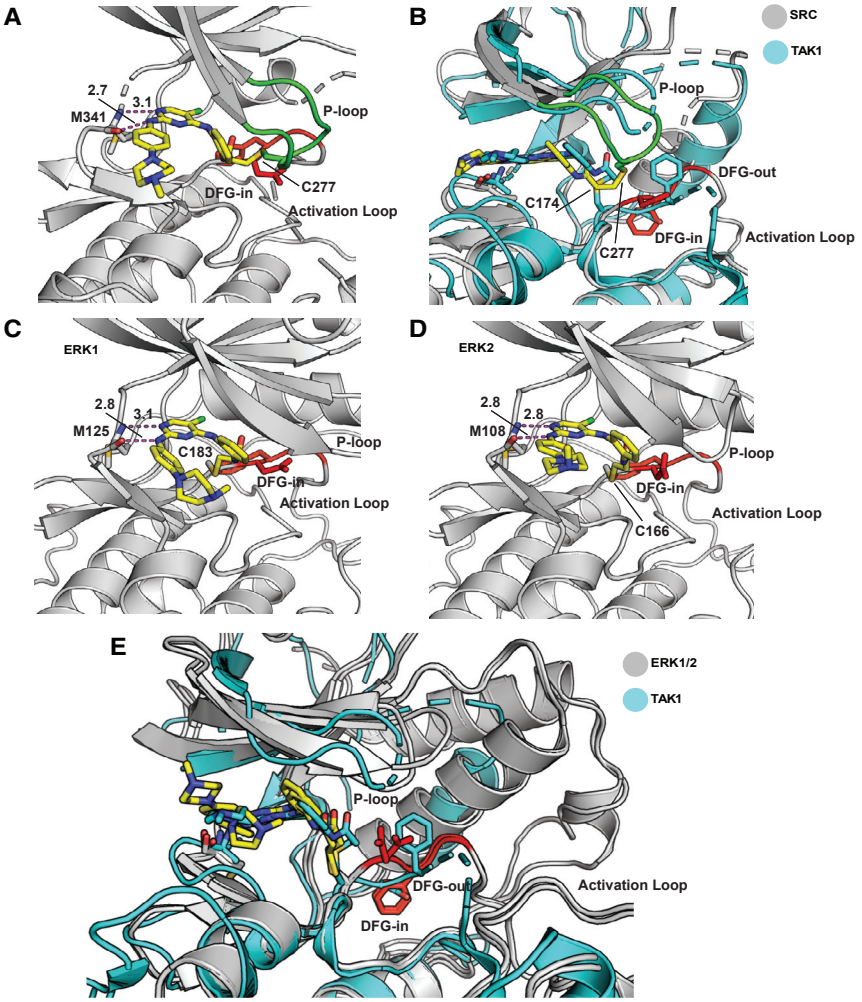

Figure 3. Crystal Structures of SRC, ERK1, ERK2, and TAK1 Bound to SM1-71 Show Interactions with Spatially Distinct Cysteines

(A) X-ray crystal structure of SRC with SM1-71 (PDB: 6ATE) forming a covalent bond with C277.

(B–D) (B) Overlay of SM1-71-bound TAK1 (PDB: 5J7S) and SRC structures show differences in the P-loop (SRC) and DFG–1 (TAK1) conformations. X-ray crystal structures of (C) ERK1 with SM1-71 (PDB: 6GES) and (D) ERK2 with SM1-71 (PDB: 6G54) forming a covalent bond with C183 and C166, respectively.

(E) Overlay of TAK1 and ERK1/2 crystal structures in complex with SM1-71 and covalent bond formation with DFG–1 cysteines.

We determined the co-crystal structure of SRC bound to SM1-71 at 2.4 Å resolution (Table S6). Covalent bond formation between the P-loop cysteine of SRC and SM1-71 was verified by MS before crystallization (PDB: 6ATE). This showed a shift in mass corresponding to an SM1-71 adduct. Proteolytic digestion showed that SM1-71 forms a covalent bond exclusively with C277 (equivalent to the C280 position in human SRC protein), located in the P-loop (Figures S5A–S5C). The cysteine 277 position is obtained from the SRC sequence from chicken, which is the organism that the viral homolog of SRC (*v-SRC*) was first identified in (Takeya et al., 1981; Anderson et al., 1985). Electron density corresponding to SM1-71 was apparent with continuous density extending toward the thiol of C277 confirming the formation of a covalent bond (Figure S5D). Similar to a previous structure of SM1-71 bound to TAK1 (PDB: 5J7S; Tan et al., 2017a), the anilinopyrimidine of SM171 formed hydrogen bonds with the backbone of M341 in the hinge region (Figure 3A) and hydrophobic interactions formed with L273, G274, V281, A293, Y340, G344, L393, and A403 (Figure S5E). In contrast to the TAK1-SM1-71 structure, the P-loop in SRC-SM171 was bent toward the active site enabling the covalent bond formation between the thiol of C277 and the acrylamide of SM1-71 (Figure 3A); in TAK1 the P-loop is disordered. Another difference is found in the activation loop: in TAK1, covalent binding of SM1-71 immediately upstream of the DFG results in an inactive "out" conformation, whereas in SRC the DFG is in an "in" conformation, which is typically the active conformation (Figure 3B).

To visualize how SMI-71 targets the DFG–1 cysteine, we determined the crystal structure of a complex with ERK1 (PDB: 6GES; Figure 3C) and ERK2 (PDB: 6F31; Figure 3D). SM1-71 adopted a type I binding mode as observed in the SRC co-complex. Interestingly, despite targeting the same DFG–1 cysteine (C183 in ERK1, C166 in ERK2, and C174 in TAK1), the inhibitor penetrated deeper into the back pocket (Figure 3E). The change in binding orientation potentially led to different trajectories of attack by the acrylamide warhead, which appears to be responsible for covalent bond formation with both DFG-in (ERK1/2) and DFG-out (TAK1) conformations. For data collection and refinement statistics, please refer to Table S6. Taken together our structural biology analysis provides useful insights toward understanding target-ligand interactions at two spatially distinct positions within the active site. They also confirm covalent target engagement toward four kinases, previously identified as covalent targets across multiple assays (Figure 4; Table S7).

In summary, 23 kinases showed covalent inhibition across at least two orthogonal assays from our analysis across seven different techniques performed under live cell, lysate, and biochemical conditions (Figure 4; Table S7). The cysteines identified across these kinases were primarily distributed within the DFG–1, P-loop, and activation loop regions (Figure 5; Table S7). Upon curation of the literature, we also noted that nine of these kinases (MAP2K4_C246, MAPKAPK5_C168, GSK3A_C262, YES1_C287, LIMK1_C349, MAP3K1_C1257, MAP2K3_C196, MAP2K6_C178, and RPS6KA3_C560) have previously not been targeted by a covalent inhibitor at these specific sites. Although, six of these have been previously labeled by covalent fragments (e.g., iodoacetamide probe) (Bak et al., 2017; Lanning et al., 2014; Backus et al., 2016; Weerapana et al., 2010; Quinti et al., 2017; Abo and Weerapana, 2015; Deng et al., 2013).

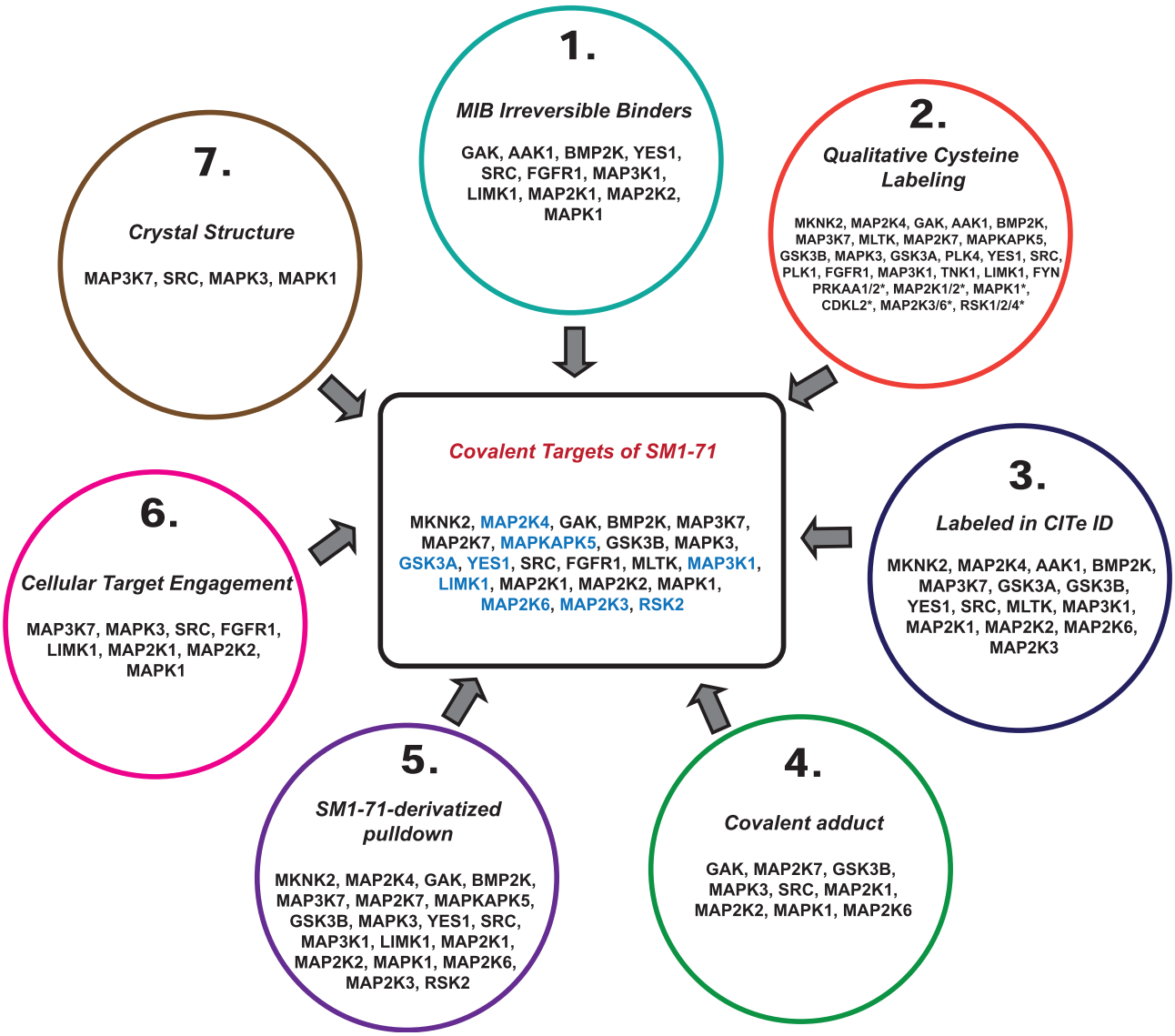

Figure 4. Snapshot of All Orthogonal Assays Performed to Elucidate and Validate Covalent Targets Inhibited by SM1-71

This schematic summarizes the list of 23 kinases covalently targeted by SM1-71, as validated by at least two orthogonal assays. Those highlighted in blue text have previously never been targeted by a covalent inhibitor before (excluding covalent fragments). Note: in the case of MIB and SM1-71-derivatized pull-down assays, we only listed kinases that overlapped with the list of covalent targets identified in one or more of the remaining assays. For the full list of targets from the MIB and SM1-71-derivatozed pull-down assays, please refer to Tables 1 and S7, respectively. *Non-unique peptides detected that mapped to multiple kinases. For a complete list, please see Table S7.

DISCUSSION

Covalent kinase inhibitors of the BTK and EGFR kinases are approved drugs in tumor types that depend on these targets. This success has stimulated the search for covalent inhibitors of other oncogenic kinases, resulting in the development of well-characterized covalent inhibitors of TEC-family kinases (BTK, ITK), RSK, FGFR, SRC, JNK, CDK7, CDK12, and CDK13 (Tan et al., 2014, 2015; Zhang et al., 2012, 2016; Kwarcinski et al., 2012; Honigberg et al., 2010; Goedken et al., 2015; Forster et al., 2016; Solca et al., 2012; Kwiatkowski et al., 2014; Zhong et al., 2015; Harling et al., 2013; Cohen et al., 2005). These inhibitors were discovered using structure-based drug design or were discovered serendipitously through inhibitor profiling. Another approach, called isoTOP-ABPP, has been utilized to scan the proteome for labeled cysteines using a cell-permeable iodoacetamide (IAA) probe (Weerapana et al., 2010). The success of this methodology has resulted in the identification of several covalently targetable proteins, previously unknown to be amenable to covalent modification. The IAA probe labels accessible cysteines, which may or may not be feasible to covalent inhibition.

In this work, we utilized a multi-targeted covalent kinase inhibitor to identify kinases that can be covalently targeted by

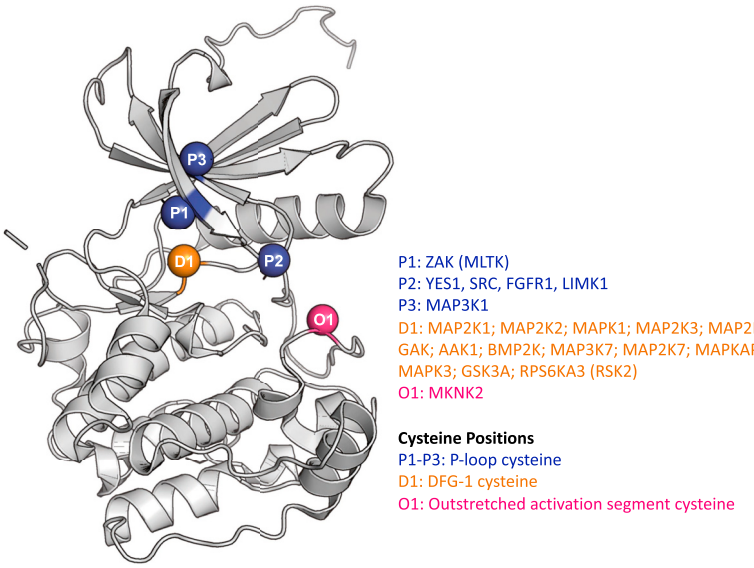

Figure 5. Ribbon-Structure Representing Cysteine Positions across the 23 Kinases Covalently Targeted by SM1-71

Through our seven different orthogonal approaches, we confirmed covalent inhibition of 23 kinases across five different spatial positions. The majority of kinases were labeled in the DFG–1 (D1) position followed by the P-loop region (P1-P3). We also identified one kinase labeled in the activation loop region (O1).

an inhibitor. We incorporated a multitude of cell-based and biochemical approaches to elucidate the targets and validate them. It is common for different profiling techniques to generate target profiles that might not completely overlap with each other. For instance, we noted that among the kinases identified as covalent targets of SM1-71 in our present study, 18 of them overlapped with the kinases identified as targets of SM1-71 in our previously published work (Tan et al., 2017b). Similarly, in our present work, we initially conducted two different chemoproteomic techniques and found that there were covalent targets identified in one that did not show up in the other. To reduce over- or underestimation of covalent targets of SM1-71, we chose to implement a suite of complementary chemoproteomic, cellular target engagement, biochemical, and structural assays. These differences typically arise from conducting experiments under varying conditions such as (1) live cells versus lysate, (2) type of affinity tag used to pull down kinases (MIBs versus SM1-71-derivatized beads), or (3) the overall workflow and analysis pipeline of techniques. Overall, from our analyses, we were able to successfully annotate covalently labeled kinases that showed irreversible inhibition in at least two of the seven orthogonal assays. Twenty-three kinases were confirmed as covalent targets of SM1-71. We further noted that 9 of the 23 kinases identified in this study have previously never been covalently targeted by a covalent inhibitor (not including covalent fragments). These findings provide ample opportunities to not only develop covalent inhibitors, but also other types of inhibitors that can potentially exploit previously unknown binding pockets offered by these kinases.

A comprehensive analysis of covalent kinase inhibitors developed to date suggests that a majority of them have been designed to inhibit cysteine residues in the front pocket (F2) of the kinase (Chaikuad et al., 2018). Kinases sharing cysteines in this position include EGFR, HER2, HER4, ITK, BTK, JAK, TEC, TKX, BLK, BMX, and MAP3K7. From our study, we observed that the most commonly labeled site was the DFG–1 cysteine, which was the original cysteine position SM1-71 was designed to target in MAP3K7 (Tan et al., 2017a). However, the ability of SM1-71 to covalently target kinases by reaching out to cysteines in the P-loop or activation loop suggests an unprecedented flexibility associated with this scaffold, capable of adopting distinct spatial conformations to interact with different cysteine residues. This was further illustrated by the co-crystal structures of SRC-SM1-71 (P-loop) and ERK1/2-SM1-71 (DFG–1). Together, these findings broaden the spectrum of kinases with conserved cysteines that can be targeted using such chemical scaffolds. We would like to emphasize that the *ortho*-position of the acrylamide warhead on SM1-71 is extremely critical. We found that when we switched the electrophile to a *meta*- or *para*-position, or further substituted SM1-71 with an *ortho*-methoxy group, there was decreased kinase binding and loss of promiscuity (data not shown). Therefore, we believe that the ability of SM1-71 to covalently/non-covalently interact with multiple kinases by assuming that different spatial orientations can be attributed to its well-positioned electrophile appended to a potent kinase inhibitor.

Our study also established a practical workflow for utilizing multi-targeted inhibitors as versatile probes to scan the kinome for covalently modifiable targets on cysteine residues. Previously, Zhao et al. (2017a) implemented a promiscuous sulfonyl fluoride-based affinity probe to scan the proteome for targets that can be covalently modified on lysine residues and identified 133 kinases within a single cell line. As another example, we utilized a multi-targeted kinase degrader, TL12-186, to successfully identify kinases most easily susceptible to ubiquitin-mediated degradation through recruitment of the E3 ligase, cereblon (Huang et al., 2018). Selective chemical probes have always served as valuable tools to address important biological questions arising from pharmacologic inhibition of selective targets or perturbation of specific signaling pathways. Through our work, and others', we have now demonstrated the utility of multi-targeted probes to reveal druggable targets within the proteome. A fundamental characteristic of most chemical probes is their ability to selectively target a specific protein of interest (Garcia-Serna and Mestres, 2011; Blagg and Workman, 2017). However, while using a multi-targeted covalent probe such as SM1-71, it is important to establish whether the compound inhibits all targets with similar potency as well as determine the mode of inhibition. First, we conducted compound-washout studies using the MIB assay to distinguish reversible from irreversible binders (Table 1). Recently, a similar study was performed using the kinobeads assay to distinguish between the

covalent and non-covalent targets of different covalent inhibitors including ibrutinib (Dittus et al., 2017). Our time-dependent evaluation of kinases, post treatment and washout, revealed strong (1) irreversible targets (e.g., GAK, SRC, YES1, MAP2K1/2, etc.) and (2) reversible targets (e.g., AURKA, PTK2, and TEC). In addition to utilizing the MIB assay to distinguish between reversible and irreversible targets, we also implemented a dose-dependent analysis using the MIB assay to calculate the IC_{50} values of target inhibition (Table S2). We further corroborated these values with IC_{50} values from a biochemical kinase assay, which strongly supported our preliminary findings for several kinases. Based on these findings, we were able to rank-order kinase targets based on their binding potency and some of the strongest binders included GAK, YES1, SRC, AAK1, LIMK1, BMP2K, AURKA, and MAP2K1/2 (IC_{50} < 10 nM in the MIB assay).

The MIB assay is a powerful technique and provides certain advantages over some of the MS-based techniques that are limited to identifying covalent targets of a compound (e.g., isoTOP-ABPP, or CITe-Id). Firstly, the MIB/kinobeads assay is a kinase-enrichment assay in which only those kinases that are not inhibited by an ATP-competitive inhibitor (reversible or irreversible) will be bound and pulled down by the beads. Another possible advantage (with caveats) is that the MIB assay is a protein-enrichment method, while other covalent capture techniques (such as isoTOP-ABPP, qualitative cysteine labeling, or CITe-Id) are based on peptide enrichment. This in turn implies that the latter techniques are limited to detecting cysteines that occur on proteotypic (MS amenable) peptides. Furthermore, if a cysteine of interest occurs on a tryptic peptide that is too long or too short, or too hydrophobic, or contains other post-translational modifications not included in the database search, the cysteine of interest will not be detected regardless of how abundant it is. However, the caveat associated with the MIB assay is that by being a protein measurement technique, it will detect numerous peptides for a large or abundant protein, and while the MS is occupied on a kinase with a lot of peptides (e.g., EPHA2, PRKDC, and SLK in our study), it may miss lower-abundant kinases (e.g., MAP3K7). However, covalent capture techniques such as CITe-Id or isoTOP-ABPP will have typically one peptide to detect per kinase and thus may be more sensitive.

Taken together, the data in this paper describe a valuable investigative tool compound to annotate druggable cysteines in kinases. Additional promiscuous scaffolds will be needed to further fully experimentally annotate which additional kinases are susceptible to covalent modification. Our work presents a comprehensive workflow involving a multi-targeted covalent kinase inhibitor and a suite of complementary techniques to validate kinases amenable to covalent inhibition. Together, these findings increase the number of kinases against which covalent inhibitors can be developed, thereby paving a way forward for covalent drug discovery initiatives.

SIGNIFICANCE

Covalent inhibitors offer key therapeutic advantages over their reversible counterparts by increasing target selectivity and inducing sustained target blockade. As a result, a lot of effort has been directed toward developing covalent kinase inhibitors, particularly those that target non-conserved cysteines within the kinome. Nearly 50% of the human kinome is amenable to covalent modification at cysteines distributed across 18 spatial locations. Despite this, the five covalent kinase inhibitors approved to date are designed to target a cysteine located within the front pocket of the kinase. Our preset study aims to address this gap, at least in part, by providing a framework involving a multi-targeted covalent kinase inhibitor and a combination of chemoproteomic and cellular assays. By systematically scanning all targetable cysteines using multiple orthogonal assays, we validate 23 kinases as being amenable to covalent modification, nine of which have previously never been targeted by a covalent inhibitor. This study illustrates a feasible workflow for identifying and validating covalent targets of compounds. Overall, we increased the number of kinases that are amenable to covalent modification in sites other than the front pocket. Together, these pave the way forward for future covalent drug discovery efforts.

STAR★METHODS

Detailed methods are provided in the online version of this paper and include the following:

- KEY RESOURCES TABLE
- CONTACT FOR REAGENT AND RESOURCE SHARING
- EXPERIMENTAL MODEL AND SUBJECT DETAILS
- METHOD DETAILS
  - Chemical Synthesis
  - Chemoproteomic Techniques
  - Cellular Target Engagement Assay
  - Cell Transfections and BRET Measurements
  - Biochemical Kinase Assay
  - Structure Determination of ERK1/2 Complexed with SM1-71
  - Purification of SRC Kinase Domain
  - Crystal Structure of SM1-71 Bound to SRC Kinase
  - Structure Determination of ERK1/2 Complexed with SM1-71
- STATISTICAL ANALYSIS
- DATA AND SOFTWARE AVAILABILITY

SUPPLEMENTAL INFORMATION

Supplemental Information can be found online at https://doi.org/10.1016/j.chembiol.2019.02.021.

ACKNOWLEDGMENTS

This work was supported by grants Welch I-1829 (to K.D.W), CPRIT RP140233 (to K.D.W.), P50-GM107618, U54HL127365, U54-CA225088, and KU-KIST Graduate School of Converging Science and Technology Program. S.R. would like to acknowledge the Jonathan M. Goldstein and Kaia Miller Goldstein Systems Pharmacology Fellowship and 3U54HL127365-02S1 (LINCS-IDG Collaboration) for supporting this work. We would like to thank HZB for the allocation of synchrotron radiation beamtime. Structural biology presented in this report are derived from work performed at Argonne National Laboratory, Structural Biology Center at the Advanced Photon Source which is operated by the University of Chicago Argonne, LLC, for the US Department of Energy, Office of Biological and Environmental Research under contract

DE-AC02-06CH11357. We thank the staff at the structural biology laboratory at UT Southwestern Medical Center and at beamline 19-ID of Advanced Photon Source, at BESSY beamline 14.2 and SLS X06SA for assistance with X-ray data collection.

AUTHOR CONTRIBUTIONS

S.R., P.K.S., and N.S.G. designed the study and wrote the manuscript with input from co-authors. Experimental work was carried out by S.R., D.G., R.A.E., C.N.B., A.C., M.S., S.B.F., and K.D.W. Compounds were synthesized by G.D. and T.L. T.S. and N.D.K. carried out docking studies. M.B. assisted with proteomics. D.G. performed SRC crystallography with assistance from S.G. K.D.W., J.A.M., and S.K. reviewed and edited the manuscript. P.K.S. (orcid.org/0000-0002-3364-1838) established the profiling platforms and co-supervised S.R., R.A.E. and M.J.B.

DECLARATION OF INTERESTS

N.S.G. is a founder, science advisory board member (SAB) and equity holder in Gatekeeper, Syros, Petra, C4, B2S, and Soltego. The Gray lab receives or has received research funding from Novartis, Takeda, Astellas, Taiho, Janssen, Kinogen, Voronoi, Her2llc, Deerfield, and Sanofi. Peter K. Sorger is a founder, SAB member, and equity holder in Merrimack Pharmaceutical and Glencoe Software; he is on the Board of Directors of Applied Biomath and the SAB of RareCyte. In the last 5 years the Sorger lab has received research funding from Novartis and Merck. Sorger declares that none of these relationships are directly or indirectly related to the content of this manuscript.

Received: October 5, 2018
Revised: December 18, 2018
Accepted: February 27, 2019
Published: April 11, 2019

REFERENCES

Abo, M., and Weerapana, E. (2015). A caged electrophilic probe for global analysis of cysteine reactivity in living cells. J. Am. Chem. Soc. *137*, 7087–7090.

Adams, P.D., Afonine, P.V., Bunkóczi, G., Chen, V.B., Davis, I.W., Echols, N., Headd, J.J., Hung, L.W., Kapral, G.J., Grosse-Kunstleve, R.W., et al. (2010). PHENIX: a comprehensive Python-based system for macromolecular structure solution. Acta Crystallogr. D Biol. Crystallogr. *66*, 213–221.

Anderson, S.K., Gibbs, C.P., Tanaka, A., Kung, H.J., and Fujita, D.J. (1985). Human cellular src gene: nucleotide sequence and derived amino acid sequence of the region coding for the carboxy-terminal two-thirds of pp60c-src. Mol. Cell. Biol. *5*, 1122–1129.

Askenazi, M., Parikh, J.R., and Marto, J.A. (2009). mzAPI: a new strategy for efficiently sharing mass spectrometry data. Nat. Methods *6*, 240–241.

Backus, K.M., Correia, B.E., Lum, K.M., Forli, S., Horning, B.D., González-Páez, G.E., Chatterjee, S., Lanning, B.R., Teijaro, J.R., Olson, A.J., et al. (2016). Proteome-wide covalent ligand discovery in native biological systems. Nature *534*, 570–574.

Bak, D.W., Pizzagalli, M.D., and Weerapana, E. (2017). Identifying functional cysteine residues in the mitochondria. ACS Chem. Biol. *12*, 947–957.

Bantscheff, M., Eberhard, D., Abraham, Y., Bastuck, S., Boesche, M., Hobson, S., Mathieson, T., Perrin, J., Raida, M., Rau, C., and Reader, V. (2007). Quantitative chemical proteomics reveals mechanisms of action of clinical ABL kinase inhibitors. Nat. Biotechnol. *25*, 1035–1044.

Blagg, J., and Workman, P. (2017). Choose and use your chemical probe wisely to explore cancer biology. Cancer Cell *32*, 268–270.

Böhm, G., Prefot, P., Jung, S., Selzer, S., Mitra, V., Britton, D., Kuhn, K., Pike, I., and Thompson, A.H. (2015). Low-pH solid-phase amino labeling of complex peptide digests with TMTs improves peptide identification rates for multiplexed global phosphopeptide analysis. J. Proteome Res. *14*, 2500–2510.

Browne, C.M., Jiang, B., Ficarro, S.B., Doctor, Z.M., Johnson, J.L., Card, J.D., Sivakumaren, S.C., Alexander, W.M., Yaron, T., Murphy, C.J., and Kwiatkowski, N.P. (2018). A chemoproteomic strategy for direct and proteome-wide covalent inhibitor target-site identification. J. Am. Chem. Soc. https://doi.org/10.1021/jacs.8b07911.

Cameron, F., and Sanford, M. (2014). Ibrutinib: first global approval. Drugs *74*, 263–271.

Chaikuad, A., Tacconi, E.M., Zimmer, J., Liang, Y., Gray, N.S., Tarsounas, M., and Knapp, S. (2014). A unique inhibitor binding site in ERK1/2 is associated with slow binding kinetics. Nat. Chem. Biol. *10*, 853–860.

Chaikuad, A., Koch, P., Laufer, S.A., and Knapp, S. (2018). The cysteinome of protein kinases as a target in drug development. Angew. Chem. Int. Ed. *57*, 4372–4385.

Chakraborty, R., Kapoor, P., Ansell, S.M., and Gertz, M.A. (2015). Ibrutinib for the treatment of Waldenström macroglobulinemia. Expert Rev. Hematol. *8*, 569–579.

Chen, V.B., Arendall, W.B., Headd, J.J., Keedy, D.A., Immormino, R.M., Kapral, G.J., Murray, L.W., Richardson, J.S., and Richardson, D.C. (2010). MolProbity: all-atom structure validation for macromolecular crystallography. Acta Crystallogr D Biol. Crystallogr *66*, 12–21.

Cohen, M.S., Zhang, C., Shokat, K.M., and Taunton, J. (2005). Structural bioinformatics-based design of selective, irreversible kinase inhibitors. Science *308*, 1318–1321.

Davids, M.S., and Brown, J.R. (2014). Ibrutinib: a first in class covalent inhibitor of Bruton's tyrosine kinase. Future Oncol. *10*, 957–967.

Deeks, E.D. (2017). Neratinib: first global approval. Drugs *77*, 1695–1704.

Deng, X., Weerapana, E., Ulanovskaya, O., Sun, F., Liang, H., Ji, Q., Ye, Y., Fu, Y., Zhou, L., Li, J., et al. (2013). Proteome-wide quantification and characterization of oxidation-sensitive cysteines in pathogenic bacteria. Cell Host Microbe *13*, 358–370.

Dittus, L., Werner, T., Muelbaier, M., and Bantscheff, M. (2017). Differential kinobeads profiling for target identification of irreversible kinase inhibitors. ACS Chem. Biol. *12*, 2515–2521.

Duncan, J.S., Whittle, M.C., Nakamura, K., Abell, A.N., Midland, A.A., Zawistowski, J.S., Johnson, N.L., Granger, D.A., Jordan, N.V., Darr, D.B., and Usary, J. (2012). Dynamic reprogramming of the kinome in response to targeted MEK inhibition in triple-negative breast cancer. Cell *149*, 307–321.

Dungo, R.T., and Keating, G.M. (2013). Afatinib: first global approval. Drugs *73*, 1503–1515.

Emsley, P., and Cowtan, K. (2004). Coot: model-building tools for molecular graphics. Acta Crystallogr. D Biol. Crystallogr. *60*, 2126–2132.

Emsley, P., Lohkamp, B., Scott, W.G., and Cowtan, K. (2010). Features and development of Coot. Acta Crystallogr. D Biol. Crystallogr. *66*, 486–501.

Eng, J.K., Mccormack, A.L., and Yates, J.R. (1994). An approach to correlate tandem mass spectral data of peptides with amino acid sequences in a protein database. J. Am. Soc. Mass Spectrom. *5*, 976–989.

Evans, P.R., and Murshudov, G.N. (2013). How good are my data and what is the resolution? Acta Crystallogr. D Biol. Crystallogr. *69*, 1204–1214.

Fedorov, O., Marsden, B., Pogacic, V., Rellos, P., Müller, S., Bullock, A.N., Schwaller, J., Sundström, M., and Knapp, S. (2007). A systematic interaction map of validated kinase inhibitors with Ser/Thr kinases. Proc. Natl. Acad. Sci. U S A *104*, 20523–20528.

Ficarro, S.B., Zhang, Y., Lu, Y., Moghimi, A.R., Askenazi, M., Hyatt, E., Smith, E.D., Boyer, L., Schlaeger, T.M., Luckey, C.J., and Marto, J.A. (2009). Improved electrospray ionization efficiency compensates for diminished chromatographic resolution and enables proteomics analysis of tyrosine signaling in embryonic stem cells. Anal. Chem. *81*, 3440–3447.

Ficarro, S.B., Zhang, Y., Carrasco-Alfonso, M.J., Garg, B., Adelmant, G., Webber, J.T., Luckey, C.J., and Marto, J.A. (2011). Online nanoflow multidimensional fractionation for high efficiency phosphopeptide analysis. Mol. Cell Proteomics *10*, O111 011064.

Ficarro, S.B., Brown, C.M., Card, J.D., Alexander, W.M., Zhang, T., Park, E., Mcnally, R., Dhe-Paganon, S., Seo, H.S., Lamberto, I., et al. (2016). Leveraging gas-phase fragmentation pathways for improved identification and selective detection of targets modified by covalent probes. Anal. Chem. *88*, 12248–12254.

Forster, M., Chaikuad, A., Bauer, S.M., Holstein, J., Robers, M.B., Corona, C.R., Gehringer, M., Pfaffenrot, E., Ghoreschi, K., Knapp, S., and Laufer, S.A. (2016). Selective JAK3 inhibitors with a covalent reversible binding mode targeting a new induced fit binding pocket. Cell Chem. Biol. *23*, 1335–1340.

Garcia-Serna, R., and Mestres, J. (2011). Chemical probes for biological systems. Drug Discov. Today *16*, 99–106.

Goedken, E.R., Argiriadi, M.A., Banach, D.L., Fiamengo, B.A., Foley, S.E., Frank, K.E., George, J.S., Harris, C.M., Hobson, A.D., Ihle, D.C., et al. (2015). Tricyclic covalent inhibitors selectively target Jak3 through an active site thiol. J. Biol. Chem. *290*, 4573–4589.

Greig, S.L. (2016). Osimertinib: first global approval. Drugs *76*, 263–273.

Harling, J.D., Deakin, A.M., Campos, S., Grimley, R., Chaudry, L., Nye, C., Polyakova, O., Bessant, C.M., Barton, N., Somers, D., et al. (2013). Discovery of novel irreversible inhibitors of interleukin (IL)-2-inducible tyrosine kinase (Itk) by targeting cysteine 442 in the ATP pocket. J. Biol. Chem. *288*, 28195–28206.

Honigberg, L.A., Smith, A.M., Sirisawad, M., Verner, E., Loury, D., Chang, B., Li, S., Pan, Z., Thamm, D.H., Miller, R.A., and Buggy, J.J. (2010). The Bruton tyrosine kinase inhibitor PCI-32765 blocks B-cell activation and is efficacious in models of autoimmune disease and B-cell malignancy. Proc. Natl. Acad. Sci. U S A *107*, 13075–13080.

Huang, H.T., Dobrovolsky, D., Paulk, J., Yang, G., Weisberg, E.L., Doctor, Z.M., Buckley, D.L., Cho, J.H., Ko, E., Jang, J., et al. (2018). A chemoproteomic approach to query the degradable kinome using a multi-kinase degrader. Cell Chem. Biol. *25*, 88–99.e6.

Hughes, C.S., Foehr, S., Garfield, D.A., Furlong, E.E., Steinmetz, L.M., and Krijgsveld, J. (2014). Ultrasensitive proteome analysis using paramagnetic bead technology. Mol. Syst. Biol. *10*, 757.

Huttlin, E.L.J., Jedrychowski, M.P., Elias, J.E., Goswami, T., Rad, R., Beausoleil, S.A., Villén, J., Haas, W., Sowa, M.E., and Gygi, S.P. (2010). A tissue-specific atlas of mouse protein phosphorylation and expression. Cell *143*, 1174–1189.

Kabsch, W. (2010). XDS. Acta Crystallogr. D Biol. Crystallogr. *66*, 125–132.

Kwarcinski, F.E., Fox, C.C., Steffey, M.E., and Soellner, M.B. (2012). Irreversible Inhibitors of c-Src kinase that target a nonconserved cysteine. ACS Chem. Biol. *7*, 1910–1917.

Kwarcinski, F.E., Brandvold, K.R., Phadke, S., Beleh, O.M., Johnson, T.K., Meagher, J.L., Seeliger, M.A., Stuckey, J.A., and Soellner, M.B. (2016). Conformation-selective analogues of dasatinib reveal insight into kinase inhibitor binding and selectivity. ACS Chem. Biol. *11*, 1296–1304.

Kwiatkowski, N., Zhang, T., Rahl, P.B., Abraham, B.J., Reddy, J., Ficarro, S.B., Dastur, A., Amzallag, A., Ramaswamy, S., Tesar, B., and Jenkins, C.E. (2014). Targeting transcription regulation in cancer with a covalent CDK7 inhibitor. Nature *511*, 616–620.

Lanning, B.R., Whitby, L.R., Dix, M.M., Douhan, J., Gilbert, A.M., Hett, E.C., Johnson, T.O., Joslyn, C., Kath, J.C., Niessen, S., et al. (2014). A road map to evaluate the proteome-wide selectivity of covalent kinase inhibitors. Nat. Chem. Biol. *10*, 760–767.

Lemeer, S., Zörgiebel, C., Ruprecht, B., Kohl, K., and Kuster, B. (2013). Comparing immobilized kinase inhibitors and covalent ATP probes for proteomic profiling of kinase expression and drug selectivity. J. Proteome Res. *12*, 1723–1731.

Levinson, N.M., and Boxer, S.G. (2014). A conserved water-mediated hydrogen bond network defines bosutinib's kinase selectivity. Nat. Chem. Biol. *10*, 127–132.

Liu, Q., Sabnis, Y., Zhao, Z., Zhang, T., Buhrlage, S.J., Jones, L.H., and Gray, N.S. (2013). Developing irreversible inhibitors of the protein kinase cysteinome. Chem. Biol. *20*, 146–159.

Mcalister, G.C., Nusinow, D.P., Jedrychowski, M.P., Wühr, M., Huttlin, E.L., Erickson, B.K., Rad, R., Haas, W., and Gygi, S.P. (2014). MultiNotch MS3 enables accurate, sensitive, and multiplexed detection of differential expression across cancer cell line proteomes. Anal. Chem. *86*, 7150–7158.

Mccoy, A.J., Grosse-Kunstleve, R.W., Adams, P.D., Winn, M.D., Storoni, L.C., and Read, R.J. (2007). Phaser crystallographic software. J. Appl. Crystallogr. *40*, 658–674.

Médard, G., Pachl, F., Ruprecht, B., Klaeger, S., Heinzlmeir, S., Helm, D., Qiao, H., Ku, X., Wilhelm, M., Kuehne, T., et al. (2015). Optimized chemical proteomics assay for kinase inhibitor profiling. J. Proteome Res. *14*, 1574–1586.

Minor, W., Cymborowski, M., Otwinowski, Z., and Chruszcz, M. (2006). HKL-3000: the integration of data reduction and structure solution–from diffraction images to an initial model in minutes. Acta Crystallogr. D Biol. Crystallogr. *62*, 859–866.

Murshudov, G.N., Skubák, P., Lebedev, A.A., Pannu, N.S., Steiner, R.A., Nicholls, R.A., Winn, M.D., Long, F., and Vagin, A.A. (2011). REFMAC5 for the refinement of macromolecular crystal structures. Acta Crystallogr. D Biol. Crystallogr. *67*, 355–367.

Cancer Discovery. (2017). Neratinib approved for HER2+ breast cancer. Cancer Discov. *7*, OF1, https://doi.org/10.1158/2159-8290.CD-NB2017-110.

Parikh, J.R., Askenazi, M., Ficarro, S.B., Cashorali, T., Webber, J.T., Blank, N.C., Zhang, Y., and Marto, J.A. (2009). multiplierz: an extensible API based desktop environment for proteomics data analysis. BMC Bioinformatics *10*, 364.

Quinti, L., Dayalan Naidu, S., Träger, U., Chen, X., Kegel-Gleason, K., Llères, D., Connolly, C., Chopra, V., Low, C., Moniot, S., et al. (2017). KEAP1-modifying small molecule reveals muted NRF2 signaling responses in neural stem cells from Huntington's disease patients. Proc. Natl. Acad. Sci. U S A *114*, E4676–E4685.

Rao, S., Du, G., Hafner, M., Subramanian, K., Sorger, P.K., and Gray, N.S. (2019). A multi-targeted probe-based strategy to identify signaling vulnerabilities in cancers. J. Biol. Chem. https://doi.org/10.1074/jbc.RA118.006231.

Shirley, M. (2018). Dacomitinib: first global approval. Drugs *78*, 1947–1953.

Singh, J., Petter, R.C., Baillie, T.A., and Whitty, A. (2011). The resurgence of covalent drugs. Nat. Rev. Drug Discov. *10*, 307–317.

Solca, F., Dahl, G., Zoephel, A., Bader, G., Sanderson, M., Klein, C., Kraemer, O., Himmelsbach, F., Haaksma, E., and Adolf, G.R. (2012). Target binding properties and cellular activity of afatinib (BIBW 2992), an irreversible ErbB family blocker. J. Pharmacol. Exp. Ther. *343*, 342–350.

Takeya, T., Hanafusa, H., Junghans, R.P., Ju, G., and Skalka, A.M. (1981). Comparison between the viral transforming gene (src) of recovered avian sarcoma virus and its cellular homolog. Mol. Cell. Biol. *1*, 1024–1037.

Tan, L., Wang, J., Tanizaki, J., Huang, Z., Aref, A.R., Rusan, M., Zhu, S.J., Zhang, Y., Ercan, D., Liao, R.G., et al. (2014). Development of covalent inhibitors that can overcome resistance to first-generation FGFR kinase inhibitors. Proc. Natl. Acad. Sci. U S A *111*, E4869–E4877.

Tan, L., Akahane, K., Mcnally, R., Reyskens, K.M., Ficarro, S.B., Liu, S., Herter-Sprie, G.S., Koyama, S., Pattison, M.J., Labella, K., et al. (2015). Development of selective covalent janus kinase 3 inhibitors. J. Med. Chem. *58*, 6589–6606.

Tan, L., Gurbani, D., Weisberg, E.L., Hunter, J.C., Li, L., Jones, D.S., Ficarro, S.B., Mowafy, S., Tam, C.P., Rao, S., et al. (2017a). Structure-guided development of covalent TAK1 inhibitors. Bioorg. Med. Chem. *25*, 838–846.

Tan, L., Gurbani, D., Weisberg, E.L., Jones, D.S., Rao, S., Singer, W.D., Bernard, F.M., Mowafy, S., Jenney, A., Du, G., et al. (2017b). Studies of TAK1-centered polypharmacology with novel covalent TAK1 inhibitors. Bioorg. Med. Chem. *25*, 1320–1328.

Ting, L., Rad, R., Gygi, S.P., and Haas, W. (2011). MS3 eliminates ratio distortion in isobaric multiplexed quantitative proteomics. Nat. Methods *8*, 937–940.

Vedadi, M., Niesen, F.H., Allali-Hassani, A., Fedorov, O.Y., Finerty, P.J., Wasney, G.A., Yeung, R., Arrowsmith, C., Ball, L.J., Berglund, H., et al. (2006). Chemical screening methods to identify ligands that promote protein stability, protein crystallization, and structure determination. Proc. Natl. Acad. Sci. U S A *103*, 15835–15840.

Weerapana, E., Wang, C., Simon, G.M., Richter, F., Khare, S., Dillon, M.B., Bachovchin, D.A., Mowen, K., Baker, D., and Cravatt, B.F. (2010). Quantitative

reactivity profiling predicts functional cysteines in proteomes. Nature *468*, 790–795.

Wu, P., Nielsen, T.E., and Clausen, M.H. (2016). Small-molecule kinase inhibitors: an analysis of FDA-approved drugs. Drug Discov. Today *21*, 5–10.

Zhang, T., Inesta-Vaquera, F., Niepel, M., Zhang, J., Ficarro, S.B., Machleidt, T., Xie, T., Marto, J.A., Kim, N., Sim, T., et al. (2012). Discovery of potent and selective covalent inhibitors of JNK. Chem. Biol. *19*, 140–154.

Zhang, T., Kwiatkowski, N., Olson, C.M., Dixon-Clarke, S.E., Abraham, B.J., Greifenberg, A.K., Ficarro, S.B., Elkins, J.M., Liang, Y., Hannett, N.M., et al. (2016). Covalent targeting of remote cysteine residues to develop CDK12 and CDK13 inhibitors. Nat. Chem. Biol. *12*, 876–884.

Zhang, J., Salminen, A., Yang, X., Luo, Y., Wu, Q., White, M., Greenhaw, J., Ren, L., Bryant, M., Salminen, W., et al. (2017). Effects of 31 FDA approved small-molecule kinase inhibitors on isolated rat liver mitochondria. Arch. Toxicol. *91*, 2921–2938.

Zhao, Q., Ouyang, X., Wan, X., Gajiwala, K.S., Kath, J.C., Jones, L.H., Burlingame, A.L., and Taunton, J. (2017a). Broad-spectrum kinase profiling in live cells with lysine-targeted sulfonyl fluoride probes. J. Am. Chem. Soc. *139*, 680–685.

Zhao, Z., Liu, Q., Bliven, S., Xie, L., and Bourne, P.E. (2017b). Determining cysteines available for covalent inhibition across the human kinome. J. Med. Chem. *60*, 2879–2889.

Zhong, Y., Dong, S., Strattan, E., Ren, L., Butchar, J.P., Thornton, K., Mishra, A., Porcu, P., Bradshaw, J.M., Bisconte, A., et al. (2015). Targeting interleukin-2-inducible T-cell kinase (ITK) and resting lymphocyte kinase (RLK) using a novel covalent inhibitor PRN694. J. Biol. Chem. *290*, 5960–5978.

Zhou, F., Sikorski, T.W., Ficarro, S.B., Webber, J.T., and Marto, J.A. (2011). Online nanoflow reversed phase-strong anion exchange-reversed phase liquid chromatography-tandem mass spectrometry platform for efficient and in-depth proteome sequence analysis of complex organisms. Anal. Chem. *83*, 6996–7005.

Zhou, F., Lu, Y., Ficarro, S.B., Adelmant, G., Jiang, W., Luckey, C.J., and Marto, J.A. (2013). Genome-scale proteome quantification by DEEP SEQ mass spectrometry. Nat. Commun. *4*, 2171.

STAR★METHODS

KEY RESOURCES TABLE

REAGENT or RESOURCE	SOURCE	IDENTIFIER
Antibodies		
Rabbit monoclonal MEK1/2	Cell Signaling Technology	Cat# 9126S; RRID: AB_331778
Mouse monoclonal ERK1/2	Cell Signaling Technology	Cat# 4696S; RRID: AB_390780
Rabbit monoclonal SRC	Cell Signaling Technology	Cat# 2123S; RRID: AB_2106047
Rabbit monoclonal TAK1	Cell Signaling Technology	Cat# 5206S; RRID: AB_10694079
Rabbit monoclonal FGFR1	Cell Signaling Technology	Cat# 9740T; RRID: AB_11178519
Rabbit monoclonal LIMK1	Cell Signaling Technology	Cat# 3842S; RRID: AB_2281332
Mouse monoclonal HRP-conjugated beta-actin	Santa Cruz Biotechnology	Cat# Sc-47778; RRID: AB_2714189
Chemicals, Peptides, and Recombinant Proteins		
Chemical Synthesis		
N-Ethyl-*N*-isopropylpropan-2-amine (DIEA)	Sigma Aldrich	Cat# D125806
2,4,5-Trichloropyrimidine	Combi-Blocks	Cat# OR-1081
Benzene-1,2-diamine	Sigma Aldrich	Cat# P23938
Tert-butyl 4-(4-aminophenyl)piperazine-1-carboxylate	Combi-Blocks	Cat# AN-1426
Acryloyl chloride	Sigma Aldrich	Cat# 549797
N-Boc-PEG2-bromide	BroadPharm	Cat# BP-22233
6-((4R,5S)-5-methyl-2-oxoimidazolidin-4-yl)hexanoic acid	Sigma Aldrich	Cat# D1411
2,4-Dichloropyrimidine	Combi-Blocks	Cat# PY-1712
4-(4-methylpiperazin-1-yl)aniline	Combi-Blocks	Cat# ST-4631
Trifluoroacetic acid	Sigma Aldrich	Cat# T6508
n-Butanol	Sigma Aldrich	Cat# 360465
s-Butanol	Sigma Aldrich	Cat# 294810
Dimethylformamide	Sigma Aldrich	Cat# 227056
Kinobeads/MIB ASSAY		
β-Mercaptoethanol	Sigma Aldrich	Cat# M7522-100ML
HEPES	VWR	Cat# J63218-AE
Sodium Chloride (NaCl)	Sigma Aldrich	Cat# S7653-250G
Triton X-100	Thermo Fisher Scientific	Cat# 28314
Ethylenediaminetetraacetic acid (EDTA)	Sigma Aldrich	Cat# E9884-100G
ethylene glycol-bis(β-aminoethyl ether)-N,N,N′,N′-tetraacetic acid (EGTA)	Sigma Aldrich	Cat# E3889-10G
Sodium Fluoride (NaF)	Sigma Aldrich	Cat# 201154-5G
Sodium Orthovanadate ($NaVO_4$)	Sigma Aldrich	Cat# S6508-10G
Tris-HCl	Sigma Adrich	Cat# T3253-100G
Dithiotretiol (DTT)	Thermo	Cat# 20290
Iodoacetemide (IAA)	Acros	Cat# 122270050
Trichloroacetic Acid (TCA)	Fisher Chemical	Cat# SA433-500
Urea	Fisher Chemical	Cat# U16-3
EPPS	Acros Organics	Cat# 172601000
LysC	Wako	Cat# 129-02541
Trypsin	Promega	Cat# V5113
Tandem Mass Tags (TMT) – 10plex	Thermo Fisher Scientific	Cat# 90406
Formic Acid	Thermo Fisher Scientific	Cat# 85178
Acetonitrile	Acros	Cat# 61001-0040

(*Continued on next page*)

Continued

REAGENT or RESOURCE	SOURCE	IDENTIFIER
Methanol	Acros	Cat# 61009-0040
Hydroxylamine	Aldrich	Cat# 467804-10ML
Ammonium Bicarbonate	Fluka	Cat# 09830-500G
CITe Id		
Glycerol	Sigma Aldrich	Cat# G5516
NP-40 (IGEPAL)	Sigma Aldrich	Cat# I8896
TCEP	Sigma Aldrich	Cat# C4706
Tris	Sigma Aldrich	Cat# T1503
Trifluoroacetic acid (TFA)	Thermo Fisher Scientific	Cat# 85183
Dual-Speed Bead Carboxylate Beads	GE Healthcare	Cat# GE65152105050250
Ammonium Hydroxide	Sigma Aldrich	Cat# 221228
Formic acid	Thermo Fisher Scientific	Cat# 28905
iTRAQ stable isotope label	Sigma Aldrich	Cat# 4352135
Streptavidin Resin	Fisher Scientific	Cat# 20359
Triethylammonium bicarbonate	Sigma Aldrich	Cat# T7408
iTRAQ 4-plex	Sigma Aldrich	Cat# 4352135
Nano-BRET		
C-terminal NanoLuc/Aurora kinase A fusion pFC32K vector	Promega	Cat# NV1041
FuGENE HD	Promega	Cat# E2311
PP384 well plate, white, flat bottom	Greiner BioOne	Cat# 781207
Transfection Carrier DNA	Promega	Cat# E4881
energy transfer probe 5	Promega	Cat# N2500
Tracer dilution buffer	Promega	Cat# N2150
NanoBRET NanoGlo Substrate	Promega	Cat# N2150
Extracellular NanoLuc Inhibitor	Promega	Cat# N2150
OptiMEM media	Thermo Scientific	Cat# 11058021
Thermal shift		
SyPRO orange dye	Invitrogen	Cat# S6650
Mx3005p machine	Agilent	https://www.agilent.com/en/product/real-time-pcr-(qpcr)/real-time-pcr-(qpcr)-instruments/mx3000p-qpcr-system-232710
Mass shift		
6230b TOF LC/MS	Agilent	https://www.agilent.com/en/products/mass-spectrometry/lc-ms-instruments/6200-series-accurate-mass-time-of-flight-(tof)-lc-ms
Mass hunter Bioconfirm B.08.00	Agilent	https://www.agilent.com/en/products/software-informatics/masshunter-suite/masshunter-for-pharma/bioconfirm-software
C3 pre-column	Agilent	Cat# 883995-909
SRC Mass Labeling and Crystal Structure		
pET28a SRC kinase expression vector	Gift from Dr. M. Seeliger (SUNY, Stony Brook)	N/A
Bacterial cells BL21DE3 cells	Gift from Dr. M. Seeliger (SUNY, Stony Brook)	N/A
Kanamycin	Sigma Aldrich	Cat# 60615
Streptomycin	Sigma Aldrich	Cat# S9137
Chloramphenicol	Sigma Aldrich	Cat# C0378
Isopropyl β-D-1-thiogalactopyranoside (IPTG)	Sigma Aldrich	Cat# 367-93-1
Glycerol	Sigma Aldrich	Cat# G5516

(*Continued on next page*)

Continued

REAGENT or RESOURCE	SOURCE	IDENTIFIER
Benzamidine	Sigma Aldrich	Cat# 618-39-3
Phenylmethylsulfonyl fluoride (PMSF)	Sigma Aldrich	Cat# 329-98-6
Profinity Ni-charged IMAC resin	Bio-Rad Laboratories	Cat# 7324612
Sodium Acetate	Sigma Aldrich	Cat# S2889
Polyethylene Glycol 3350	Hampton Research	Cat# HR2-591
ERK1/2 Crystal Structure		
Escherichia coli Rosetta	Novagen	Cat# 70954
pNIC28-Bsa4 plasmids encoding ERK1	Structural genomics consortium (SGC)	N/A
pNIC28-Bsa4 plasmids encoding ERK2	Structural genomics consortium (SGC)	N/A
PEG 4000	Molecular dimension	Cat# MD2-250-11
Lithium sulfate	Molecular dimension	Cat# MD2-250-45
Citrate buffer	Molecular dimension	Cat# MD2-022
5-iodotubercidin	Sigma	Cat# I100
XDS	Kabsch, 2010	http://xds.mpimf-heidelberg.mpg.de/
aimless	Evans and Murshudov, 2013	http://www.ccp4.ac.uk
PHASER	Mccoy et al., 2007	http://www.ccp4.ac.uk
COOT	Emsley et al., 2010	http://www.ccp4.ac.uk
REFMAC5	Murshudov et al., 2011	http://www.ccp4.ac.uk
Molprobity	Chen et al., 2010	http://molprobity.biochem.duke.edu/
Critical Commercial Assays		
SelectScreen™ Biochemical Kinase Profiling	Thermo Fisher Scientific	N/A
Experimental Models: Cell Lines		
Human: H23 lung adenocarcinoma (male)	Pasi Janne (Dana Farber Cancer Institute, Boston, MA)	N/A
Human: Calu6 lung adenocarcinoma (female)	Pasi Janne (Dana Farber Cancer Institute, Boston, MA)	N/A
HEK-293T (Apirat)	ATCC	ATCC CRL-3216
Software and algorithms		
GraphPad Prism 7.0	GraphPad Software 7825 Fay Avenue, Suite 230 La Jolla, CA 92037 USA	www.graphpad.com
Deposited Data		
SRC-SM1-71	https://www.rcsb.org (this study)	6ATE
ERK1-SM1-71	https://www.rcsb.org (this study)	6GES
ERK2-SM1-71	https://www.rcsb.org (this study)	6G54
SRC-Bosutinib	https://www.rcsb.org (Levinson and Boxer, 2014)	4MXO
Starting model for phasing for ERK1	https://www.rcsb.org (Chaikuad et al., 2014)	4QTA
Starting model for phasing for ERK2	https://www.rcsb.org (Chaikuad et al., 2014)	4QTB
Other		
RPMI-1640 media	ATCC	Cat# 30-2001
Fetal Bovine Serum (Heat Inactivated)	Gibco	Cat# 10438-026
Penicillin/Streptomycin	Corning	Cat# 30-002
Phosphate Buffered Saline, 1X	Corning	Cat# 21040CV
Trypsin (0.25%)	Corning	Cat# 25053CI

(*Continued on next page*)

Continued

REAGENT or RESOURCE	SOURCE	IDENTIFIER
HALT Protease and Phosphatase Inhibitor Cocktail (100X)	Thermo Fisher Scientific	Cat# 78446
M-PER™ Mammalian Protein Extraction Reagent	Thermo Fisher Scientific	Cat# 78505
4x Laemmli Sample Buffer	Bio-Rad	Cat# 1610747
20X Tris Buffered Saline	Santa Cruz Biotechnology	Cat# sc-362305
10X Tris/Glycine/SDS buffer	Bio-Rad	Cat# 161-0772
10X Transfer Buffer	Bio-Rad	Cat# 35040
SuperSignal West Dura Extended Duration Substrate	Thermo Fisher Scientific	Cat# 34076
Nonfat dry milk	Cell Signaling Technology	Cat# 9999S
Any kD Mini-PROTEAN TGX Precast Protein Gels (10-well or 15-well)	Bio-Rad	Cat# 4569034, Cat# 4569036
Micro BCA Protein Assay Kit	Thermo Fisher Scientific	Cat# 23235
Solid Phase Extraction (SPE) cartridges	Thermo Fisher Scientific	Cat# 60109-001
Pierce High pH Reversed-Phase Peptide Fractionation Kit	Thermo Fisher Scientific	Cat# 84868
SYPRO™ Orange Protein Gel Stain	Thermo Fisher Scientific	Cat# S6650

CONTACT FOR REAGENT AND RESOURCE SHARING

Further information and requests for resources and reagents should be directed to and will be fulfilled by the Lead Contact, Nathanael Gray (Nathanael_Gray@dfci.harvard.edu).

EXPERIMENTAL MODEL AND SUBJECT DETAILS

Cell lines used in the study included NSCLC cells H23-KRAS^{G12C} and Calu-6-KRAS^{Q61K} that were a generous gift from Dr. Pasi Janne [Dana Farber Cancer Institute (DFCI), Boston, MA]. Cell lines were tested for mycoplasma contamination (Lonza MycoAlert Kit Cat. # LT07-318) and authenticated using short tandem repeat (STR) profiling (Molecular Diagnostics Laboratory, DFCI, Boston, MA). Cells were maintained in RPMI-1640 media (ATCC, 30-2001). All media were supplemented with 10% heat-inactivated fetal bovine serum (Gibco) and 1% penicillin/streptomycin (30-002-CI, Corning). Cells were grown in incubators maintained at 37°C and 5% CO_2. The sex of these cell lines is irrelevant to our study.

METHOD DETAILS

Chemical Synthesis

Detailed methodology on the synthesis of compounds has been previously described (Tan et al., 2017a, 2017b). Additional information can be found in Data S1.

Chemoproteomic Techniques

1. Multiplexed Inhibitor Beads Assay in H23 Cells/Lysate

H23-KRAS^{G12C} cells were grown in 15 cm dishes and collected by rinsing twice with cold PBS and scraping/collecting by adding 1 mL cold PBS substituted with 100X HALT protease and phosphatase inhibitor cocktail (final concentration 1X) (Thermo Fisher Scientific, 78446). Collected cells were then centrifuged at 1500 rpm at 4°C for 10 min and stored at -80°C until future use. In case of the washout experiment, cells were treated with 1 μM SM1-71 or SM1-71-R or DMSO for 4h, after which they were rinsed twice with PBS, replaced with fresh media and collected at different times (0h, 2h, 4h, 6h and 24h) following compound-washout. Collected cells were centrifuged at 1500 rpm at 4°C for 10 min and stored at -80°C until future use. Frozen cell pellets were lysed using the MIB lysis buffer (50 mM HEPES pH 7.5, 150 mM NaCl, 0.5% Triton X-100, 1 mM EDTA, 1 mM EGTA, 10 mM NaF, 2.5 mM $NaVO_4$), sonicated briefly and centrifuged at 4000 rpm for 15 min at 4°C. Lysate was clarified by sequentially passing through a 0.45 μm filter and a 0.22 μm filter, aliquoted into 2 mL protein low-binding tubes and frozen at -80°C. Protein quantification was carried out using the Micro BCA Protein Assay Kit (23235, Thermo Fisher Scientific) and 3 mg of each sample was further subjected to the MIB assay. In case of the MIB dose-dependent kinase inhibition assay, 3 mg aliquots of multiple samples were pre-treated with 0.001, 0.01, 0.1, 0.5, 1, 5 and 10 μM of SM1-71 or DMSO with overnight incubation at 4°C with end-to-end rocking. In both MIB assays performed (probe-washout and dose-dependent inhibition), each sample (e.g. each dose or treatment condition) was subjected to kinase enrichment by passing sequentially through a set-up consisting of columns packed with sepharose beads

(200 μL/column) and the multiplexed inhibitor beads (MIBs) (350 μL/column). The MIBs were a generous gift from Dr. Gary Johnson (Department of Pharmacology, University of North Carolina) (Duncan et al., 2012). Alternating washes were performed with high/low salt MIB wash buffers (50 mM HEPES pH 7.5, 150 mM NaCl for low and 1 mM NaCl for high, 0.5% Triton X-100, 1 mM EDTA, 1 mM EGTA) followed by a wash with 0.1% (w/v) SDS containing low salt MIB wash buffer. Kinases bound by the MIBs were eluted twice using 500 μL/column of MIB elution buffer (0.5% w/v SDS, 1% v/v β-mercaptomethanol, 0.1M Tris-HCl pH 6.8). The collected eluate was boiled for 15 min at 97°C and collected into protein low-binding tubes. The collected samples were reduced with cold 1M Dithiotreitol (DTT) (5 μL/1mL sample) and incubated at 56°C for 30 min. Samples were then alkylated using 30 μL/1mL sample of 0.5 M iodoacetamide (IAA) and incubated at RT for 30 min. Samples were then precipitated with tricholoracetic acid (25% final volume), washed twice with methanol and evaporated. Following this step, they were solubilized with 8M urea in 20mM EPPS and further diluted with 30 μL 20 mM EPPS to bring the final concentration of urea to 4 M, at which point 0.5 μL of lysC (2 μg/μl) was added to each sample and incubated at room temperature (RT) for 16h. After this, the urea concentration was further diluted to 1.6M by addition of 90 μL 20 mM EPPS and 2 μL trypsin (0.5 μg/μL) was added to each sample and incubated at 37°C for 6h. Acetonitrile was added to each sample (3 μL) followed by addition of 3 μL of tandem mass tag (TMT) labels. After 1h incubation at RT, 10 μL from each sample was combined and diluted with 100 μL 1% formic acid and passed through stage tips for desalting. The sample was eluted with 70% acetonitrile/1% formic acid, evaporated, reconstituted in 3% acetonitrile/5% formic acid and injected on to the mass spectrometer to perform a QC check on sample mixing and TMT labeling. After this quality control step, the reaction was quenched with hydroxylamine (final volume 1%) for 10 mins at RT. Samples were then combined, diluted with 100% formic acid, centrifuged and the supernatant was collected and further diluted with 3x 1% formic acid prior to passing through a solid phase extraction (SPE) cartridges (60109-001, Thermo Fisher Scientific) step for desalting. Following this, the sample was eluted with 70% acetonitrile/1% formic acid, evaporated and reconstituted with 300 μL 50 mM ammonium bicarbonate. Finally, the sample was fractionated using the Pierce High pH Reversed-Phase Peptide Fractionation Kit (84868, Thermo Fisher Scientific), passed through stage tips, eluted with 70% acetonitrile/1% formic acid, evaporated and reconstituted with 3% acetonitrile/5% formic acid before injecting into the mass spectrometer. Each fraction was loaded onto a 100 μm id, 35 cm long column packed with 1.8 μm beads (Sepax, Newark DE) and separated using a 3h gradient from 8-27% B, where buffer B was 99% ACN and 1% FA and buffer A was 96% water, 3% ACN and 1% FA using an Easy 1000 nano-LC (Thermo-Fisher Scientific, San Jose, CA). All MS analyses were performed on an Orbitrap Fusion Lumos mass spectrometer (Thermo) using a multi-notch MS3 method (Ting et al., 2011, Mcalister et al., 2014). Raw data was converted to mzXML and searched via Sequest (Eng et al., 1994) version 28 against a concatenated Uniprot database downloaded 02/04/2014. Variable modifications of oxidized Methionine and over-labeling of TMT on Serine, Threonine and Tyrosine (Böhm et al., 2015) were considered. Linear discriminate analysis (Huttlin et al., 2010) was used to distinguish forward and reverse hits and reverse hits were filtered to an FDR of 1% at the protein level. Shared peptides were collapsed into the minimally sufficient number of proteins using rules of parsimony. Quantitation filters of > 185 sum reporter ion S:N and > 0.7 isolation specificity were incorporated. Dose-response/time-dependent curves were plotted using the GraphPad Prism 7.0 software.

2. Qualitative Labeling of Cysteines Modified by SM1-71

Cell pellets from H23-KRAS^{G12C} or Calu-6-KRAS^{Q61K} cells were lysed with NP-40 lysis buffer (50 mM Tris pH 7.5, 150 mM NaCl, 1 mM EDTA, 10% v/v glycerol, 0.5% v/v NP-40, 1 mM TCEP, protease inhibitors). Sample was precleared with streptavidin resin for 1h at 4°C. The supernatant was treated with 2 μM of SM1-71-DTB at 4°C for 18 h. Sample was diluted 1:1 with 8 M urea, 50 mM Tris pH 8 and reduced with 10 mM DTT for 30 min at 56°C then alkylated with 20 mM IAA for 30 min at RT. Sample was further diluted to 2 M urea with pH 8 lysis buffer before trypsin digestion at 37°C overnight. Streptavidin resin was added to the sample and incubated at RT for 1 h. The resin was sequentially washed with 3x with lysis buffer, 3x with PBS, and finally 2x with water. Peptides were eluted with 50% acetonitrile (MeCN), 0.1% trifluoroacetic acid (TFA) and concentrated by vacuum centrifugation. Peptides were cleaned using the SP3 paramagnetic bead methodology (Hughes et al., 2014). Briefly, dual-Speed Bead Carboxylate Beads (GE Healthcare) were added to peptides reconstituted in 95% MeCN and allowed to bind for 10 min at RT. Beads were washed with MeCN before peptides eluted in 100 mM Ambic, 2% DMSO and vacuum dried before final reconstitution in 5% DMSO, 100 mM ammonium formate for RP-SAX-RP LC-MS/MS. Detailed descriptions of this methodology are provided elsewhere (Zhou et al., 2013). Peptides were automatically fractionated across first and second dimension high-pH reversed phase and high-pH strong anion exchange chromatographic stages. Peptides were gradient eluted from the third dimension (low-pH RP) into a Q-Exactive HF mass spectrometer (ThermoFisher Scientific, San Jose, CA) using a 90-min organic gradient (5-50% B in 90 min, A = 0.1% FA, B = acetonitrile with 0.1% FA). The electrospray voltage was set at 3.2 kV. A top-15 data-dependent method was used for precursor selection and MS/MS. A normalized collision energy of 37 eV was used. Native .RAW data files from the mass spectrometer were processed using our multiplierz Python-based framework (Parikh et al., 2009; Askenazi et al., 2009) to generate .mgf files for input to Mascot (Matrix Science). MS/MS spectra were charge reduced, deisotoped, and processed to remove peaks corresponding to inhibitor fragmentation as described previously (Ficarro et al., 2016). The following m/z values corresponding to fragmentation of DGY-03-146 were removed from all MS/MS spectra: 346.233, 197.128, 240.168, 422.185, 528.249, 614.231, 767.412, 853.41, 855.412, 857.41, 879.40, and 896.41. Peptide precursor masses were recalibrated on a per-scan basis by correcting all m/z values based on accurate mass recorded for the $Si(CH_3)_2O_6$ peak in each spectrum. All data were searched against a forward-reverse human database assembled from the NCBI Refseq database. For de-isotoped HCD spectra, the precursor mass tolerance was set to 10 ppm and the MS/MS fragment ion tolerance was set to 25 mmu. Search parameters included trypsin specificity, with a maximum of two missed cleavages, fixed carbamidomethylation of Cys, variable oxidation on Met, variable deamidation of Asn and Gln, and variable

DGY-03-146 labeling of Cys (+993 Da, allowing neutral loss of 993 Da). Reported peptide sequences were filtered based on a 1% FDR. A list of cysteine sites labeled by SM1-71-DTB was generated from this list of identified peptides.

3. Covalent Inhibitor Target Site Identification (CITe-Id)

H23-KRAS^{G12C} cells were treated with DMSO or increasing concentrations of SM1-71 for 2 h at 37°C. Cells were harvested and washed with PBS before lysis with NP-40 lysis buffer (50 mM Tris pH 7.5, 150 mM NaCl, 1 mM EDTA, 10% v/v glycerol, 0.5% v/v NP-40, 1 mM TCEP, protease inhibitors) and lysate clearance centrifugation. Protein concentration was determined by BCA. Samples were precleared with streptavidin resin for 1 h at 4°C. The supernatant was treated with 2 μM of SM1-71-DTB and incubated at 4°C for 18 h. Protein was precipitated in the presence of dual-Speed Bead Carboxylate Beads (GE Healthcare) as described by Hughes et al.(Hughes et al., 2014) Precipitated proteins were washed sequentially with 70% ethanol and acetonitrile (MeCN) again. Additionally, the flow-through and washes were re-precipitated at -20°C for 1 hr. and after repeating the previous washes was added to the bead precipitated protein and re-solubilized with 100 mM ammonium bicarbonate (ambic). Samples were reduced with 10 mM DTT for 30 min at 56°C. Samples were then alkylated with 20 mM IAA for 30 min at RT before trypsin digestion at 37°C overnight. Streptavidin resin was added to the samples and incubated at RT for 1 h. The beads were sequentially washed with lysis buffer, PBS, and water. Peptides were eluted with 50% MeCN, 0.1% trifluoroacetic acid (TFA). Samples were vacuum dried. Samples were resuspended in 30% 0.5M TEAB, 70% EtOH and iTRAQ reagent was added and allowed to incubate at RT for 1 h. Samples were then combined and acidified before vacuum drying. Peptides were cleaned using the peptide cleanup protocol from Hughes et al. (Hughes et al., 2014) Briefly, Carboxylate Beads were added to peptides reconstituted in 95% MeCN. Beads were washed with MeCN before peptides eluted in 100 mM ambic, 2% DMSO and vacuum dried. Samples were reconstituted in 5% DMSO, 100 mM ammonium formate for RP-SAX-RP LC-MS/MS. Detailed descriptions of the multidimensional chromatography system are provided elsewhere(Zhou et al., 2011, 2013; Ficarro et al., 2011). Peptides were automatically fractionated across first and second dimension high-pH reversed phase and high-pH strong anion exchange chromatographic stages. Peptides were gradient eluted from the third dimension (low-pH RP) into a Q-Exactive HF mass spectrometer (ThermoFisher Scientific) using a 90 min organic gradient (5-60% B in 90 min., A = 0.1% FA, B = acetonitrile with 0.1% FA). The electrospray voltage was set at 3.5 kV. A top-15 data-dependent method was used for precursor selection and MS/MS. The normalized collision energy was set to 37 eV. Data was processed as described for the qualitative cysteine labeling experiment. The same set of inhibitor-specific fragment ions were removed from MS/MS spectra(Ficarro et al., 2016). In addition to the previously described modifications, fixed iTRAQ 4-plex labeling on Lys and N-termini (+144 Da) was included for searching the data. Normalized reporter ion signal for labeled cysteine residues from multiple PSMs was summed and a log2 ratio was generated for each reporter channel by comparing it to the DMSO-treated control channel. Inhibitor concentrations and log2 ratios were used to generate a trendline for each labeled site with the y-intercept set to zero. The slope of this trendline became the competitive dose response for the cysteine site.

4. Thermal Shift and Mass Shift Assays

The Tm shift assays and data evaluation for melting temperatures were performed according to the protocol previously described (Fedorov et al., 2007). In brief, the protein at 2 μM was mixed with 10 μM inhibitor in the presence of SyPRO orange dye (Invitrogen). The fluorescence spectrum was measured using a Real-Time PCR Mx3005p machine (Stratagene). Kinases at 0.12 mM in 10 mM HEPES, pH 7.5, 500 mM NaCl were incubated with 0.2 mM SM1-71 at 4°C for 4 hrh and 24 h. The proteins at 10 μl were diluted with 0.1% formic acid (80 μl), and were injected into C3 pre-column in the LC/MS system. The desalted eluant was ionized in positive mode with 120 volts and injected into time-of-flight (ESI-TOF) mass spectrometry. Intact mass was determined by deconvolution using Mass hunter Bioconfirm software.

5. SM1-71-Derivatized Beads Pulldown

H23-KRAS^{G12C} cell lysate (1 mg protein) was incubated with 1 μM of SM1-71 or equivalent volume of DMSO overnight at 4°C with end-to-end rocking. Henceforth, all incubation and wash steps consisted of end-to-end rocking. 200 μL of N-Hydroxysuccinimidyl-Sepharose 4 Fast Flow beads (Sigma Aldrich) were washed with an amine-free buffer [20 mM EPPS (pH 8)] and reconstituted in 100 μL 20 mM EPPS to get a final volume of 150-200 μL. Washed beads were coupled with equal volume of 2 mM SM1-71-Peg-NH_2 (SM1-71 linked to primary amine) by incubating overnight at 4°C. Unbound drug was removed by washing with 20 mM EPPS and the reaction was quenched for 45 min at RT with 100 mM ammonium bicarbonate followed by washing with 20 mM EPPS. Once the beads were activated and ready to use, they were incubated with H23 cell lysate pretreated with SM1-71 or DMSO for 1h at RT. To remove weakly/reversibly bound kinases, beads were repeatedly washed with 200 μL 2% SDS containing lysis buffer with intermittent shaking on a heat block (50-60°C). In addition, beads were washed twice with 200 μL of 8M urea and reconstituted with 200 μL of 1.6 M urea in 20 mM EPPS solution and further diluted with 250 μL 20 mM EPPS. Samples were then digested with trypsin (4 μL) overnight at RT and acidified using 4.5 μL of 100% formic acid to get a final concentration of 1% formic acid. Samples were desalted and cleaned up using a Sep-Pak, eluted with 70% acetonitrile /1% formic acid solution and evaporated. They were reconstituted with 40 μL 20 mM EPPS and 5 μL 100% acetonitrile prior to labeling with tandem mass tag (TMT) labels for 1h at RT. The reaction was quenched with 0.5 μL hydroxylamine (1% final volume) and the samples were combined, acidified with 1μL 100% formic acid (final volume 1%) and further diluted with 300 μL of 1% formic acid. The combined sample was centrifuged (12,000 rpm, 10 min) and the supernatant was passed through the Sep-Pak step to desalt. The sample was eluted with 70% acetonitrile/1% formic acid and reconstituted in 50 mM ammonium bicarbonate after evaporation. The sample was then fractionated, passed through stage tips for cleaning up/desalting, eluted with 70% acetonitrile/1% formic acid, evaporated and reconstituted with 3% acetonitrile/5% formic acid before injecting into the mass spectrometer. Samples were analyzed by LC/MS3 as described above (*vide supra*).

Cellular Target Engagement Assay

H23-KRAS^{G12C} cells were treated with 1 μM of SM1-71, SM1-71 or DMSO for 2h, followed by compound-washout and replacement with fresh media. Cells were then collected by rinsing twice with ice-cold PBS and lysed 0h, 2h and 4h post-washout using the M-PER lysis buffer (78505, Thermo Fisher Scientific) substituted with 1X HALT protease and phosphatase inhibitor (78446, Thermo Fisher Scientific). Samples were then incubated with TL-13-68 (SM1-71-biotin) overnight at 4°C with constant rotation. A part of the lysate was collected to detect total protein levels (inputs) and the remaining lysate was subjected to pulldown using streptavidin agarose resin (20353, Thermo Fisher Scientific). Proteins pulled down the beads were washed 5-6 times using ice-cold M-PER. Beads from each of the samples were then dried, mixed with 4X Laemmli Sample Buffer (1610747, Bio-Rad), substituted with 5% β-mercaptoethanol (Sigma Aldrich), boiled at 95°C for 10 min. SDS-electrophoresis was carried out using the Any kD Mini-PROTEAN TGX Precast Protein Gels (4569034, 4569036 Bio-Rad). Transfer was carried out using PVDF membranes (0.45 μm pore size, Novex Life Technologies) and 5% nonfat dry milk (9999S, Cell Signaling Technology) in 1X Tris Buffered Saline (TBS) (sc-362305, Santa Cruz Biotechnology) substituted with 0.1% Tween solution was used as the blocking buffer and to prepare antibody solutions. The 10X running (Tris/Glycine/SDS buffer, 161-0772, Biorad), 10X transfer (35040, Thermo Fisher Scientific) and 20X TBS (sc-362305, Santa Cruz) buffers were diluted to 1X solutions prior to use. Antibodies were purchased from Cell Signaling Technology for MEK1/2 (9126S - rabbit), ERK1/2 (4696S - mouse), SRC (2123S - rabbit), TAK1 (5206S-rabbit), FGFR1 (9740-T - rabbit) and LIMK1 (3842S – rabbit) diluted to a final concentration of 1:1000 (primary) or 1: 10,000 (secondary). Beta-actin antibody was obtained from Santa Cruz (sc-47778 - mouse) and diluted to a final concentration of 1:5000. Blots were visualized by adding 1:1 ratio of SuperSignal West Dura Extended Duration Substrate (34076, Thermo Fisher Scientific) and scanning them using the myECL imager (Thermo Fisher Scientific). Two independent experiments were carried out and bands from one of the experiments have been represented in Figure 2.

Cell Transfections and BRET Measurements

C-terminal NanoLuc/Aurora kinase fusion, encoded in pFC32K expression vectors (Promega), was used. For cellular BRET target engagement experiments, HEK-293T were transfected with NLuc/target fusion constructs using FuGENE HD (Promega) according to the manufacturer's protocol. Briefly, Nluc/target fusion constructs were diluted into Transfection Carrier DNA (Promega) at a mass ratio of 1:10 (mass/mass), diluted with OptiMEM media to a twentieth part of the volume of the HEK cells. FuGENE HD was added at a ratio of 1:3 (μg DNA: μL FuGENE HD). One part (vol) of FuGENE HD complexes was combined with 20 parts (vol) of HEK-293 cells suspended at a density of 2 x 10^5 cells/ml and afterwards the mixture was incubated in a humidified, 37°C/5% CO_2 incubator for 24 h. After this, the cells were washed and resuspended in OptiMEM. For Target engagement assays 4 x 10^3 cells/well were plated out on a white 384-well plate (Greiner). Kinetic studies required preincubation of cells with compound of roughly 10 x the half inhibitory concentration over two hours with a cell density of 5 x 10^5 cells/ml. After this, the medium was exchanged with OptiMEM and cell suspension was plated out on 96-well plate with a final volume of 90 μl. For all experiments energy transfer probe 5 (Promega) was used in triplicates at a concentration of 0,1 μM, diluted to a 20x working concentration with tracer dilution buffer (12.5 mM HEPES, 31.25% PEG-400, pH 7.5). Starting point of the kinetic measurement was upon adding of the experiments energy transfer probe 5, NanoBRET NanoGlo Substrate and Extracellular NanoLuc Inhibitor (Promega) according to the manufacturer's recommended protocol. In contrast to the kinetic measurements, compounds and the energy transfer probe were added to the cells and incubated for 2h in humidified, 37°C/5% CO_2 incubator. The chemical inhibitors were prepared as concentrated stock solutions in DMSO (Sigma-Aldrich) and diluted with OptiMEM for this experiment. Straight before the measurement NanoGlo Substrate and Extracellular NanoLuc Inhibitor (Promega) were mixed carefully with the supernatant. In both cases luminescence was measured on a TecanSpark equipped with 450 nm BP filter (donor) and 600 nm LP filter (acceptor) using 0.5 s integration time. For kinetic measurements a kinetic loop of 60s was applied. Milli-BRET units (mBU) are calculated by multiplying the raw BRET values by 1000.

$$mBU = \frac{1000 * I[600\ nm]}{I[450\ nm]}$$

Inhibitory constants were calculated by using the sigmoidal dose-response (three parameters) equation in GraphPad Prism.

$$Y = Bottom + \frac{Top - Bottom}{1 + 10^{(X - LogIC50)}} \quad \text{(Equation 1)}$$

Apparent kinetics were estimated by applying the one phase association equation to the normalized kinetic data (Equation 2).

$$Y = Y0 + (Plateau - Y0) * (1 - \exp(-K * x)) \quad \text{(Equation 2)}$$

Biochemical Kinase Assay

Kinase inhibition was commercially assessed using the SelectScreen™ Biochemical Kinase Profiling Service (Thermo Fisher Scientific). These assays are based on the principle of time-resolved fluorescence resonance energy transfer (TR-FRET) and can measure the IC_{50} of a compound to inhibit a given kinase.

Structure Determination of ERK1/2 Complexed with SM1-71

ERK1 and ERK2 protein was prepared as previously described (Chaikuad et al., 2014). For ERK1, the complexed crystals with SM1-71 were achieved by ligand substitution soaking of the initial 5-iodotubercidin-ERK1 complexed crystals, obtained by sitting drop vapor diffusion crystallization using 33% PEG4000, 0.1 M Tris pH 8.0 and 0.2 M lithium sulfate, with 10 mM SM1-71. Co-crystallization of ERK2 was performed in a sitting drop at 4°C using reservoir solution containing 0.9 M lithium sulfate, 0.5 M ammonium sulfate and 0.1 M citrate at pH 5.9. The crystals cryoprotected with mother liquor supplemented with 20-30% ethylene glycol were initially tested for diffraction quality at BESSY beamline 14.2, while the complete data were then collected at SLS X06SA using the wavelength of 1.0000 Å. The data were processed and scaled with XDS (Kabsch, 2010) and aimless(Evans and Murshudov, 2013), respectively. Structure solution was obtained by molecular replacement using the program Phaser (Mccoy et al., 2007) and the published coordinates of ERK1 and ERK2 (PDB; 4QTB and 4QTA). Iterative cycles of manual model building alternated with maximum likelihood refinement were performed in COOT (Emsley et al., 2010) and REFMAC (Murshudov et al., 2011), respectively. The final models were validated for their geometric correctness using Molprobity (PMID: 20057044). Data collection and refinement statistics are given in Table S6.

Purification of SRC Kinase Domain

The SRC kinase domain was purified as reported previously (Kwarcinski et al., 2016) with minor modifications. pET28a containing SRC kinase domain (residues 251–533) fused with a TEV protease cleavable N-terminal 6×-His tag, a gift from M. Seeliger (SUNY, Stony Brook), was introduced into YGT cells (BL21DE3 cells transformed with YopH on a Streptomycin resistant plasmid and GroEL/TriggerFactor on a ChlorAmphenicol resistant plasmid). Cells were grown in LB media supplemented with kanamycin, streptomycin and chloramphenicol at 37°C until an OD_{600} of ~ 0.8 then induced with 0.5 M IPTG for 12 h at 16°C. Cells were harvested by centrifugation at 3000 x g for 10 min at 4°C and stored at -80°C until purification. Cells were harvested by centrifugation at 3000 x g for 10 min at 4°C and stored at -80°C until purification. Cell pellets were resuspended in buffer-A (50 mM Tris pH 8.0, 500 mM NaCl, 10 mM imidazole, 5 mM β-ME and 5 %glycerol) supplemented with protease inhibitors benzamidine (15 μg/ml) and PMSF (1mM) and lysed with four cycles of homogenization at 8000 psi in ice using EmulsiFlex-C3 homogenizer (AVESTIN, Inc. ON, Canada). Lysate was clarified by centrifugation at 18000 rpm, 4°C for 1 h. Supernatant was collected and filtered through a 0.22-μm filter and loaded on to 5 ml Bio-Scale Mini cartridges filled with Profinity Ni-charged IMAC resin (Bio-Rad Laboratories, Inc, California, USA). After washing for 10 column volumes, His-tagged SRC kinase was eluted with buffer-B (50 mM Tris pH 8.0, 500 mM NaCl, 300 mM imidazole, 5 mM β-ME and 5 % glycerol) and desalted into buffer-C (50 mM Tris pH 8.0, 50 mM NaCl, 5 mM β-ME and 5 % glycerol). Typical protein yield was 30 mg/liter. His-tag was removed using TEV protease at a ratio of 1:20 relative to SRC kinase overnight at 4°C. Final purification of SRC kinase was performed using size exclusion chromatography in buffer-D (50 mM Hepes pH 7.5, 100 mM NaCl, 2 mM DTT and 5% glycerol).

Crystal Structure of SM1-71 Bound to SRC Kinase

The SRC kinase domain was concentrated to 10 mg/ml, mixed with SM1-71 in a 1:2 molar ratio and incubated for 1 h at room temperature before crystallization. Crystals were obtained by hanging drop vapor diffusion at 20°C (100 mM MES pH 6.5, 14-20 % PEG 3350, 350-420 mM Sodium Acetate). Thin sheets initially appeared in two days and were used for microseeding to obtain diffraction quality crystals. Crystals were harvested and frozen in liquid nitrogen prior to data collection using 20% glycerol as cryoprotectant. Diffraction data was collected using beamline 19-ID of the Advanced Photon Source, Argonne National Laboratory and scaled using HKL3000 (Minor et al., 2006). Molecular replacement solution was obtained using Phaser (Mccoy et al., 2007) and 4MXO (Levinson and Boxer, 2014) as initial search model. Model building and refinement was carried out using Coot (Emsley and Cowtan, 2004) and Phenix (Adams et al., 2010). Data collection and refinement statistics are given in Table S6.

Structure Determination of ERK1/2 Complexed with SM1-71

ERK1 and ERK2 protein was prepared as previously described (Chaikuad et al., 2014). For ERK1, the complexed crystals with SM1-71 were achieved by ligand substitution soaking of the initial 5-iodotubercidin-ERK1 complexed crystals with 10 mM SM1-71 for one month using the method described previously (Chaikuad et al., 2014). Crystallization was performed in a sitting drop at 4°C using reservoir solution containing 0.9 M lithium sulfate, 0.5 M ammonium sulfate and 0.1 M citrate at pH 5.9. The crystals cryoprotected with mother liquor supplemented with 20-30% ethylene glycol were initially tested for diffraction quality at BESSY beamline 14.2, while the complete data were then collected at SLS X06SA using the wavelength of 1.0000 Å. The data were processed and scaled with XDS (Kabsch, 2010) and aimless(Evans and Murshudov, 2013), respectively. Structure solution was obtained by molecular replacement using the program Phaser (Mccoy et al., 2007) and the published coordinates of ERK1 and ERK2 (Chaikuad et al., 2014). Iterative cycles of manual model building alternated with refinement were performed in COOT (Emsley et al., 2010) and REFMAC (Murshudov et al., 2011), respectively. Data collection and refinement statistics are given in Table S6.

STATISTICAL ANALYSIS

All statistical details can be found described in the Method Details section of the STAR Methods. GraphPad Prism 7.0 software was used to carry out statistical analysis.

DATA AND SOFTWARE AVAILABILITY

The authors declare that data supporting the findings in this study are available within the paper and the supplementary files submitted. If additional information is required, it can be made available upon request. Accession codes are found in supplemental files describing proteins identified in chemoproteomic assays. The co-crystal structures of SRC-SM1-71, ERK1-SM1-71 and ERK2-SM1-71 are deposited in PDB under the codes 6ATE, 6GES and 6G54, respectively.

Cell Chemical Biology, Volume *26*

Supplemental Information

Leveraging Compound Promiscuity to Identify Targetable Cysteines within the Kinome

Suman Rao, Deepak Gurbani, Guangyan Du, Robert A. Everley, Christopher M. Browne, Apirat Chaikuad, Li Tan, Martin Schröder, Sudershan Gondi, Scott B. Ficarro, Taebo Sim, Nam Doo Kim, Matthew J. Berberich, Stefan Knapp, Jarrod A. Marto, Kenneth D. Westover, Peter K. Sorger, and Nathanael S. Gray

SUPPLEMENTARY FIGURES

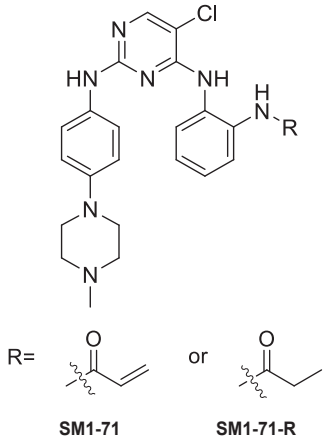

Figure S1: Chemical structure (*related to Table-1, figures 1-5*). SM1-71 and its reversible analogue, SM1-71-R.

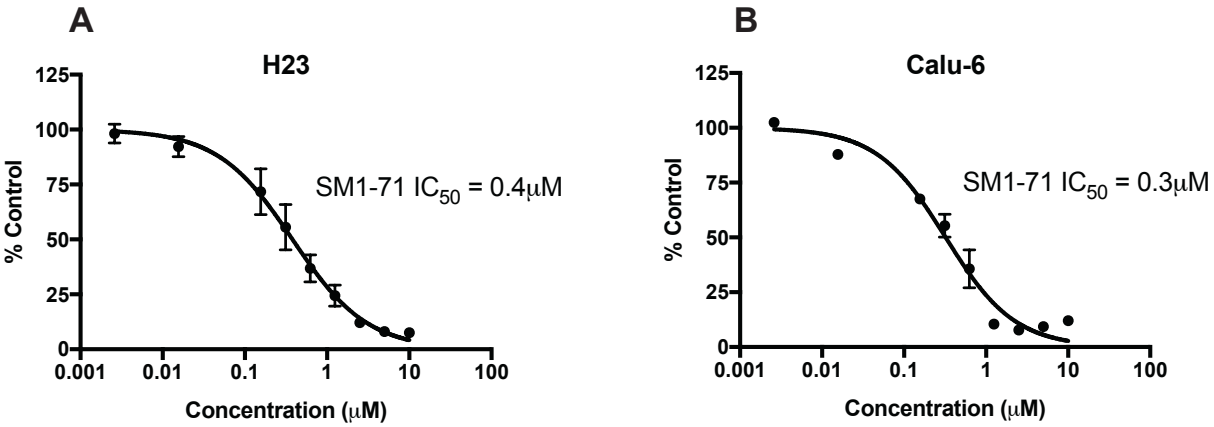

Figure S2: Growth inhibition assay in H23 and Calu-6 non-small cell lung cancer cell lines (*related to Table-1*). (a) H23-KRAS^{G12C} and **(b)** Calu-6-KRAS^{Q61K} cells were treated with various concentrations of SM1-71 for a period of 72h followed by measurement of cell viability using CellTiter-Glo. Dose-response curves were generated and the corresponding IC_{50} values were calculated using the GraphPad Prism 7.0 software.

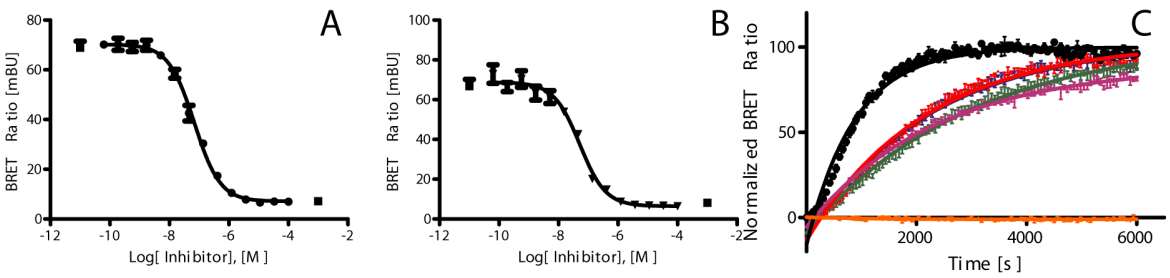

Figure S3: NANOBret™ assay measuring target engagement and binding kinetics of SM-71 and SM-71-R towards AURKA in HEK293T cells (*related to Table-1*). Target engagement of **(a)** SM1-71 and **(b)** SM1-71-R towards AURKA, as determined against a fluorescent-labeled tracer molecule on full-length AURKA. **(c)** Relative off-rates of SM1-71 (blue), SM1-71-R (green) and control compounds VX680 (red) and danusertib (magenta) at 0.5 µM on AURKA.

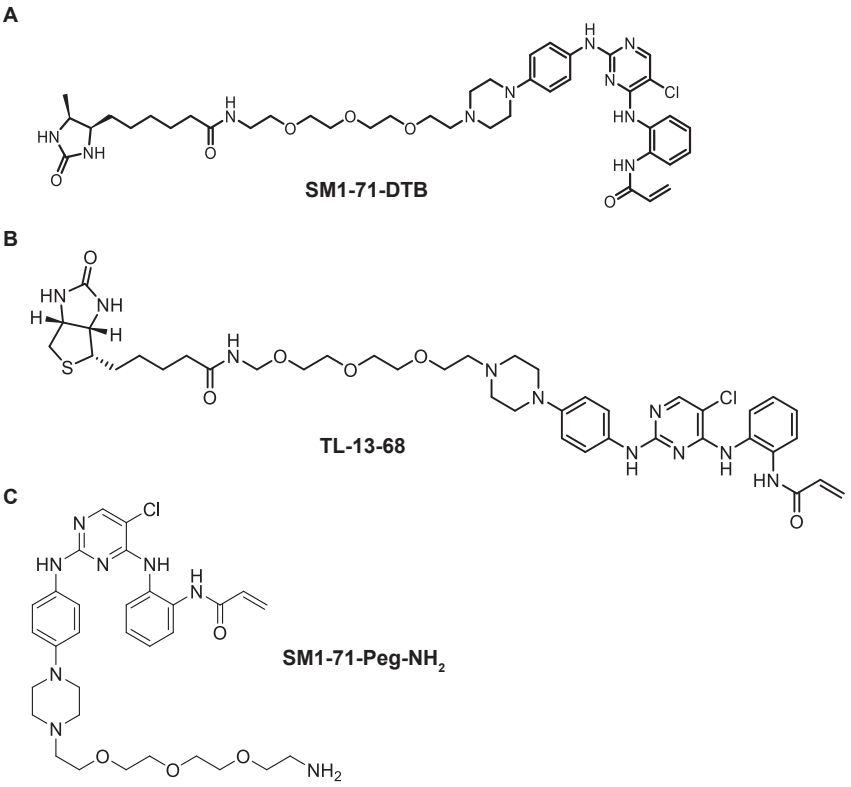

Figure S4: Chemical structures (*related to figures 1, 2 and 4*). (A) Desthiobiotin-tagged version of SM1-71 used in the qualitative cysteine labeling and Covalent Inhibitor Target site Identification (CITe Id) experiments. **(B)** Biotin-tagged version of SM1-71, TL13-68 used in the cellular target engagement assay. **(C)** Compound used to conjugate N-Hydroxysuccinimidyl-Sepharose beads in the affinity-based enrichment assay.

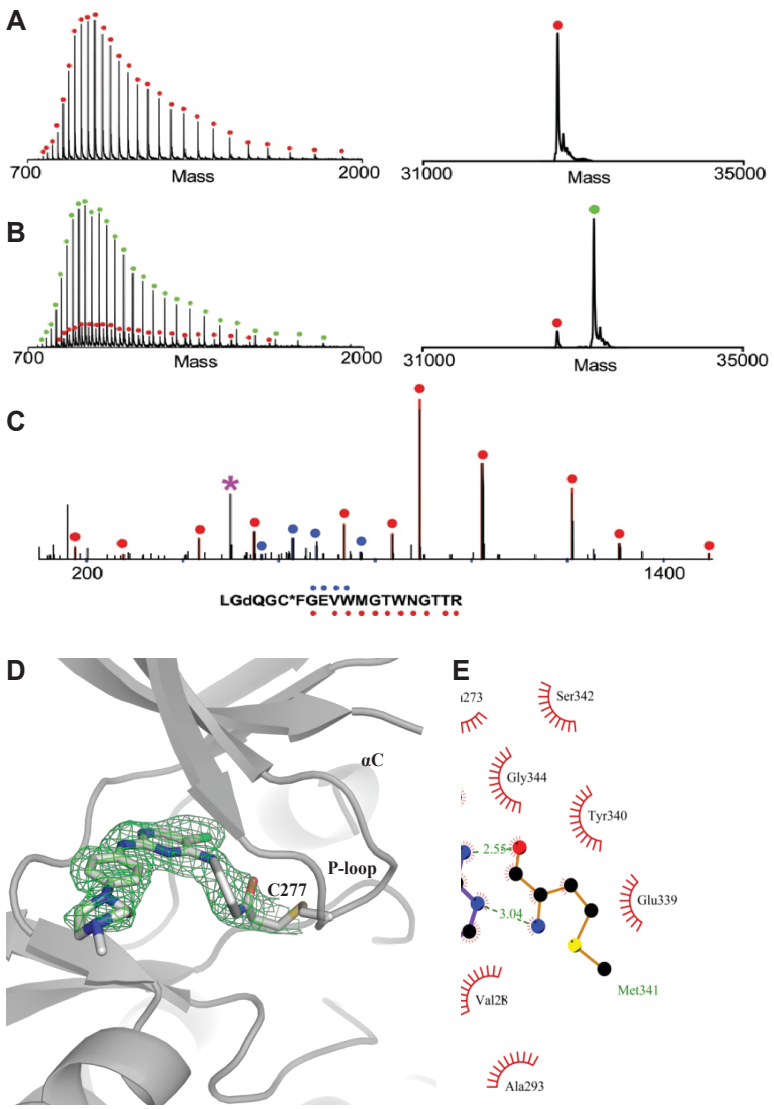

Figure S5. **Analysis of SM1-71-SRC adduct formation by mass spectrometry and characteristics of SM1-71 binding to SRC (*related to figure 3*). (A, B)** Mass spectra (left) and zero-charge mass spectra (right) for SRC treated with DMSO **(A)** or SM1-71 **(B)**. Peaks derived from unmodified protein are labeled with red circles, and peaks derived from SM1-71 modified protein are labeled with green circles. The mass shift after treatment corresponds to the covalent addition of a single SM1-71 molecule to the protein. **(C)** MS/MS spectrum acquired during CE-MS analysis of tryptic peptides from SM1-71 treated protein. Ions of type b and y are indicated by blue and red glyphs, respectively. C*, SM1-71 modified cysteine residue; dQ, deamidated glutamine; Purple * indicates SM1-71 thiolated ion. **(D)** Electron density (F_o-F_c map contoured at

2.5σ; green mesh) for SM171 extends to C277 in the p-loop of SRC kinase. **(E)** Interactions of SM1-71 with active site residues of SRC kinase. Hydrogen bonds are in dashed lines (green) and hydrophobic contacts are shown in red spokes.

SUPPLEMENTARY TABLES

Table S1 (*related to Table-1*): List of kinases inhibited by SM1-71 in the MIB assay

Gene	Description
GAK	Cyclin-G-associated kinase
MAP2K2	Dual specificity mitogen-activated protein kinase kinase 2
YES1	Tyrosine-protein kinase Yes
MAP2K1	Dual specificity mitogen-activated protein kinase kinase 1
AURKA	Aurora kinase A
AAK1	AP2-associated protein kinase 1
SRC	Isoform 2 of Proto-oncogene tyrosine-protein kinase Src
BMP2K	BMP-2-inducible protein kinase
LIMK1	LIM domain kinase 1
MAP3K1	Mitogen-activated protein kinase kinase kinase 1
ACVR1	Activin receptor type-1
MAPK1	Mitogen-activated protein kinase 1
TEC	Tyrosine-protein kinase Tec
FGFR1	Isoform 21 of Fibroblast growth factor receptor 1
PKMYT1	Membrane-associated tyrosine- and threonine-specific cdc2-inhibitory kinase
WEE1	Wee1-like protein kinase
LYN	Tyrosine-protein kinase Lyn
PTK2	Isoform 5 of Focal adhesion kinase 1
PIK3C3	Phosphatidylinositol 3-kinase catalytic subunit type 3
ACVR1B	Isoform 4 of Activin receptor type-1B
CDK9	Isoform 2 of Cyclin-dependent kinase 9
STK16	Serine/threonine-protein kinase 16
IGF1R	Insulin-like growth factor 1 receptor
PIK3R4	Phosphoinositide 3-kinase regulatory subunit 4
PIP5K1A	Isoform 3 of Phosphatidylinositol 4-phosphate 5-kinase type-1 alpha
INSR	Insulin receptor
HCK	Tyrosine-protein kinase HCK
TGFBR2	Isoform 2 of TGF-beta receptor type-2
MARK2	Isoform 14 of Serine/threonine-protein kinase MARK2
CDK13	Cyclin-dependent kinase 13

TK2	Thymidine kinase 2, mitochondrial
CSNK2A1	Casein kinase II subunit alpha
FYN	Tyrosine-protein kinase Fyn
PRKDC	DNA-dependent protein kinase catalytic subunit
TGFBR1	Isoform 2 of TGF-beta receptor type-1
CSNK1G1	Casein kinase I isoform gamma-1
CSNK1A1	Casein kinase 1, alpha 1, isoform CRA_g
DDR1	Isoform 4 of Epithelial discoidin domain-containing receptor 1
MET	Hepatocyte growth factor receptor
CSNK1D	Casein kinase I isoform delta
CDK17	Cyclin-dependent kinase 17
PRKD3	Serine/threonine-protein kinase D3
EPHA10	Ephrin type-A receptor 10
CSNK1E	Casein kinase I isoform epsilon
EPHB2	Ephrin type-B receptor 2
MAP3K11	Mitogen-activated protein kinase kinase kinase 11
EPHA2	Ephrin type-A receptor 2
MAPK3	Mitogen-activated protein kinase 3
PIP4K2C	Phosphatidylinositol 5-phosphate 4-kinase type-2 gamma
TNIK	TRAF2 and NCK-interacting protein kinase
AGK	Acylglycerol kinase, mitochondrial
CSNK1G3	Isoform 4 of Casein kinase I isoform gamma-3
PAK4	Serine/threonine-protein kinase PAK 4
EIF2AK3	Eukaryotic translation initiation factor 2-alpha kinase 3

Table S2 (*related to Table-1)*: Kinase inhibitory potency (IC_{50}-nM) determined by MIB and biochemical kinase assays

Kinase	**MIB_SM1-71**	**Biochemical_SM1-71**	**Biochemical_SM1-71-R**
GAK	0.8	0.9	60.5
MAP2K2	9.3	30.8	1260
YES1	0.8	2.5	8.3
MAP2K1	10.4	83.1	2740
AAK1	4.4	11.4	17
SRC	2	3.8	23.2
BMP2K	7.1	/	/
LIMK1	5.4	27.1	622
MAP3K1	28.7	/	/
MAPK1	48.3	1320	>10000

FGFR1	/	54.2	64
PIK3C3	/	>10000	/
PIK3R4	/	/	/
AURKA	10.3	3.7	2.7
ACVR1	/	64	/
CSNK2A1	>10000	/	/
DDR1	8400	/	/
MET	10000	228	171
EPHA10	>10000	/	/
CSNK1E	>10000	/	/
EPHB2	>10000	/	/
EPHA2	>10000	/	/
PIP4K2C	>10000	/	/
AGK	>10000	/	/
EIF2AK3	/	/	/
PKMYT1	>10000	/	/
CDK9	>10000	/	/
STK16	>10000	/	/
IGF1R	600	207	169
PIP5K1A	>10000	/	/
INSR	767	/	/
TGFBR2	577	276	/
CDK13	>10000	/	/
CSNK1G1	>10000	/	/
CDK17	>10000	/	/
PRKD3	166	/	/
MAP3K11	>10000	/	/
MAPK3	107	2820	/
TEC	31.8	186	109
LYN	187	/	/
PTK2	36.4	37.1	32.3
HCK	/	/	/
TGFBR1	>10000	/	/
WEE1	145	/	/
ACVR1B	>10000	/	/
MARK2	135.5	/	/
TK2	>10000	/	/
FYN	/	65.5	/
PRKDC	>10000	/	/

CSNK1A1	>10000	/	/
CSNK1D	>10000	/	/
TNIK	6919	/	/
CSNK1G3	>10000	/	/
PAK4	>10000	/	/

Table S3 (*related to figure 4*): Thermal shift assay across kinases with temperature shifts reported

Kinase	**Thermal Shift (∘C)**
GAK	24.4
MKK7	21.7
STK6	17.1
MAP2K6	16.3
MAP2K1	15.7
MAP2K2	14.9
BMP2K	13.6
ABL1	10.9
AAK1	10.6
FGFR3	10
RPS6KA5	9.3
JNK1	8.8
MAPK1 (ERK2)	8.5
CLK1	8.4
MAPK3 (ERK1)	8
GSK3B	7.9
JNK3	7.9
BTK	7.8
JNK2	7.1
CHEK2	6.8
SRC	6.5
FGFR2	5.7
STK38L	5.5
FGFR1	4.9
FGFR4	4.6
CLK3	4.4
EPHA2	3.4
PRKC2	2.6
CSNK2A1	2.4

MAPK6	2.3
PKMYT1	2.2
PAK1	2.1
EPHB4	2
PRKG2	1.8
PRKCN	1.2
CDK2	1.1
PRKCM	0.9
STK39	0.7
p38 alpha	0.5
Pim1	0.4
Pim3	0.4
PDK4	-0.9
VRK1	-2.8

Table S4 (*related to figure 4*): Summary of mass spectrometry analyses of the covalent adducts between SM1-71 and selected kinases

Kinase	start (0h)	Mass Shift	4h	Mass Shift	24h	Mass Shift	Covalent Adduct
AAK1	39039.4	native	39039.5	no	39039.2	no	NO
BMP2K	34754.4	native	34754.3	no (75%)	34754.2	no (~40%)	potential moderate affinity
			35218.2	463.9 (~25%)	35218.1	463.9	
						(~60%)	
MAPK1	41477.4	native	41941.1	463.7 (complete)	41941.3	463.9 (complete)	YES
FGFR1	37537.2	native	37536.4	no	37536.6	no (~65%)	potential weak interaction
					38000.4	463.8	
						(~15%)	
	37715.2	phos (2)	37714.4	no	37714.5	no (~15%)	
					38178.7	464.2	
						(~5%)	
FGFR2	38362.8	native	38362.4	no (~75%)	38362.8	no (~50%)	potential weak interaction
				463.6 (~5%)	38826.6	463.8	
						(~25%)	

	38540.7	phos (2)	38540.3	no (~20%)	38540.6	no (~20%)	
					39004.6	464	
						(~5%)	
FGFR3	35271.1	native	35271.1	no (>95%)	35271.1	no (~80%)	potential weak interaction
					35735	463.9	
						(~20%)	
FGFR4	34841	native	34840.8	no (~80%)	34840.9	no (~40%)	potential moderate interaction
			35304.6	463.8	35304.8	463.9	
				(~20%)		(~60%)	
SRC	31724.65	native	32188.31	463,1 (complete)	32188.53	463,44 (complete)	YES
MAPK3 (ERK1)	43223.36	native	43686.69	463.33 (complete)	43687.33	463.97 (complete)	YES
MAP2K6	35393.35	native	35856.86	463.32 (~60%)	35857.25	463.48 (~60%)	YES
	35473.56	phos (1)	35936.84	463.28 (~40%)	35937.33	463.77 (~40%)	
MAP2K1	37725.22	native	37727.44	no (~20%)	37726.58	no (~90%)	YES
			38191.56	464.12 (~80%)	38190.93	463.42 (90%)	
MAP2K2	44511.6	native	44975.6	464.0 (complete)	44975.7	464.1 (complete)	YES
MAP2K7	34889.54	native	34889.72	no (~5%)	34890.19	no (~5%)	YES
			35353.75	464.21 (~95%)	35354.28	464.74 (~93%)	
					35818.08	928.54 (~2%)	
MAP2K7 C202S	37339.65	native	37803.12	463,47 (complete)	37802.95	463,3 (>95%)	YES
					38267.14	927.49 (<5%)	
GAK	38137.63	native	38601.33	463.7 (complete)	38601.47	463.84 (complete)	YES
GSK3B	41551.41	native	41552.2	no			YES
	41631.56	phos (1)	41632.22	no			(moderate affinity)
			42016.09	464.68 (~25%)	42016.48	465.07 (~50%)	
			42096.09	464.53 (~25%)	42096.48	464.92 (~50%)	
ABL1	33077.04	native	33077.35	no	33077.18	no	NO
BTK	32906.17	native	32906.37	no	32906.61	no (>90%)	unlikely
					33370.5	464.33 (<10%)	(extremely weak affinity)

CLK1	39516.9	native	39517.11	no	39516.87	no	NO
	39597.04	phos (1)	39597.17	no	39596.99	no	
	39676.93	phos (2)	39677.02	no	39676.89	no	
CLK3	42251.12	native	42250.91	no	42250.95	no	NO
CSNK2A1	40262.97	native	40263.46	no (~90%)	40264.36	no (~75%)	potential weak interaction
			40727.13	464.16 (<10%)	40728.19	465.22 (~25%)	
EPHA2	34419.33	native	34419.66	no	34419.5	no	NO
JNK1	41998.74	native	41999.12	no	41999.66	no	NO
JNK2	41377.02	native	41376.72	no	41379.58	no	NO
JNK3	42091.74	native	42092.52	no	42093.53	no	NO
MAPK6	36238.11	native	36237.68	no	36238.09	no	unlikely
					36701.22	463.13 (<5%)	(extremely weak affinity)
RPS6KA5	37279.52	native	37279.14	no	37278.57	no	NO
	37360.36	phos (1)	37360.07	no	37359.34	no	
STK6	32897.4	native	32897.2	no	32897.3	no	NO

Table S5 (*related to figure 4*): List of kinases showing at least 1.5-fold inhibition in the affinity-based enrichment assay using SM1-71-derivatized beads (detection by mass spectrometry)

Kinase	**Description**	**Fold-inhibition**
MAP2K1	MP2K1_HUMAN Dual specificity mitogen-activated protein kinase kinase 1	18.8
MAP2K2	MP2K2_HUMAN Dual specificity mitogen-activated protein kinase kinase 2	18.1
SRC	SRC_HUMAN Isoform 2 of Proto-oncogene tyrosine-protein kinase Src	6.9
MAP2K6	MP2K6_HUMAN Dual specificity mitogen-activated protein kinase kinase 6	6.3
MAP2K3	MP2K3_HUMAN Isoform 2 of Dual specificity mitogen-activated protein kinase kinase 3	5.8
LIMK1	LIMK1_HUMAN LIM domain kinase 1	5.5
MKNK2	MKNK2_HUMAN MAP kinase-interacting serine/threonine-protein kinase 2	4.7
MAPKAPK5	MAPK5_HUMAN MAP kinase-activated protein kinase 5	3.9
MAP2K5	MP2K5_HUMAN Dual specificity mitogen-activated protein kinase kinase 5	3.8
MAPK1	MK01_HUMAN Mitogen-activated protein kinase 1	3.7
GAK	GAK_HUMAN Cyclin-G-associated kinase	3.6

MAP2K7	MP2K7_HUMAN Isoform 2 of Dual specificity mitogen-activated protein kinase kinase 7	3.5
TK1	K7ERV3_HUMAN Thymidine kinase	3.4
PASK	PASK_HUMAN PAS domain-containing serine/threonine-protein kinase	3.3
MAPK3	MK03_HUMAN Mitogen-activated protein kinase 3	3.3
AURKA	A3KFJ0_HUMAN Aurora kinase A	3.3
NADK	NADK_HUMAN Isoform 2 of NAD kinase	3.2
TK1	KITH_HUMAN Thymidine kinase, cytosolic	3.2
CHKA	CHKA_HUMAN Choline kinase alpha	3.0
PKM	KPYM_HUMAN Pyruvate kinase PKM	2.8
AURKA	AURKA_HUMAN Aurora kinase A	2.8
MAP2K4	MP2K4_HUMAN Isoform 2 of Dual specificity mitogen-activated protein kinase kinase 4	2.6
MAP3K7	M3K7_HUMAN Isoform 1A of Mitogen-activated protein kinase kinase kinase 7	2.6
DTYMK	KTHY_HUMAN Thymidylate kinase	2.6
YES1	YES_HUMAN Tyrosine-protein kinase Yes	2.4
ITPK1	ITPK1_HUMAN Inositol-tetrakisphosphate 1-kinase	2.4
RPS6KA3	KS6A3_HUMAN Ribosomal protein S6 kinase alpha-3	2.1
MAP3K1	M3K1_HUMAN Mitogen-activated protein kinase kinase kinase 1	2.1
DSTYK	DUSTY_HUMAN Dual serine/threonine and tyrosine protein kinase	2.1
TTK	TTK_HUMAN Dual specificity protein kinase TTK	1.9
ITPKC	IP3KC_HUMAN Inositol-trisphosphate 3-kinase C	1.9
WNK1	WNK1_HUMAN Isoform 5 of Serine/threonine-protein kinase WNK1	1.8
PBK	TOPK_HUMAN Lymphokine-activated killer T-cell-originated protein kinase	1.8
GSK3B	GSK3B_HUMAN Isoform 2 of Glycogen synthase kinase-3 beta	1.8
STYK1	STYK1_HUMAN Tyrosine-protein kinase STYK1	1.8
MELK	MELK_HUMAN Maternal embryonic leucine zipper kinase	1.8
CSNK1G1	KC1G1_HUMAN Casein kinase I isoform gamma-1	1.7
EPHA3	EPHA3_HUMAN Ephrin type-A receptor 3	1.7
BMP2K	BMP2K_HUMAN BMP-2-inducible protein kinase	1.7
GK5	GLPK5_HUMAN Putative glycerol kinase 5	1.6
ALPK1	ALPK1_HUMAN Alpha-protein kinase 1	1.6
CLK4	CLK4_HUMAN Dual specificity protein kinase CLK4	1.6
CAMK1D	KCC1D_HUMAN Calcium/calmodulin-dependent protein kinase type 1D	1.6
STK17B	ST17B_HUMAN Serine/threonine-protein kinase 17B	1.6
CHEK2	CHK2_HUMAN Isoform 9 of Serine/threonine-protein kinase Chk2	1.6
RIOK3	RIOK3_HUMAN Serine/threonine-protein kinase RIO3	1.6
CHEK1	CHK1_HUMAN Serine/threonine-protein kinase Chk1	1.5
CAMKK1	KKCC1_HUMAN Isoform 2 of Calcium/calmodulin-dependent protein kinase kinase 1	1.5

STK10	STK10_HUMAN Serine/threonine-protein kinase 10	1.5
PCK2	PCKGM_HUMAN Phosphoenolpyruvate carboxykinase [GTP], mitochondrial	1.5
WEE1	WEE1_HUMAN Wee1-like protein kinase	1.5

Table S6 (*related to figures 3 and 4*): Data collection and refinement statistics for SRC-SM1-71, ERK1-SM1-71 and ERK2-SM1-71 crystal structures

Data collection	**SRC-SM1-71**
X-ray source	APS 19–1D
Wavelength (Å)	0.979
Space group	P 21 21 21
Unit cell	
a, b, c (Å)	41.51, 62.76, 105.89
α, β, γ (°)	90.0, 90.0, 90.0
Resolution (Å)	50.00 - 2.40 (2.44 - 2.40)[a]
Unique reflections	10,914
Redundancy	9.9 (2.5)
Completeness (%)	96.0 (73.7)
Wilson B-factor	45.31
Rmerge (%)	9.3 (44.8)
I/σ	21.05 (1.4)
Refinement	
Resolution	40.47 - 2.40 (2.44 - 2.40)
Reflections Used	10,871
Rfree reflections	544
Rwork/Rfree (%)	19.3/22.8
Non-hydrogen atoms	2155
Protein	2058
Water	64
Ligand	33
RMSD	
Bond lengths (Å)	0.002
Bond angles (°)	0.506
Average B-factor (Å2)	62.07
Protein	62.19
Ligands	71.62
Water	53.38
Ramachandran plot (%)	
Favored	95.55

Allowed	4.05
Disallowed	0.4
PDB accession code	6ATE
Data collection	**ERK2-SM1-71**
PDB IDs	6G54
Data collection	
Space group	P 3221
Cell dimensions	
a, b, c (Å)	91.8, 91.8, 99.3
α, β, γ (°)	90.0, 90.0, 120.0
Resolution (Å)	49.65-2.05 (2.12-2.05)
Rmerge	0.057 (0.911)
CC(1/2)	0.999 (0.783)
I /σI	16.1 (2.0)
Completeness (%)	100.0 (100.0)
Redundancy	7.9 (8.0)
Refinement	
No. reflections	30,813 (2,978)
Rwork / Rfree	0.183/ 0.221
No. atoms	
Protein	2,854
Compound	33
Water and solvents	258
B factors (Å2)	
Protein	56
Compounds (SM1-71)	58
Water and solvents	58
r.m.s. deviations	
Bond lengths (Å)	0.013
Bond angles (°)	1.3
Data collection	**ERK1-SM1-71**
PDB IDs	6GES
Data collection	
Space group	P 21
Cell dimensions	
a, b, c (Å)	62.0, 94.0, 64.9
α, β, γ (°)	90.0, 91.8, 90.0
Resolution (Å)	47.02-2.07 (2.13-2.07)
Rmerge	0.061 (0.786)
CC(1/2)	0.999 (0.799)

I /σI	13.5 (2.0)
Completeness (%)	98.9 (99.3)
Redundancy	5.4 (5.4)
Refinement	
No. reflections	44,884 (3,496)
Rwork / Rfree	0.170/ 0.213
No. atoms	
Protein	5,708
Compound	66
Water and solvents	375
B factors (Å2)	
Protein	45
Compounds (SM1-71)	71
Water and solvents	51
r.m.s. deviations	
Bond lengths (Å)	0.014
Bond angles (°)	1.4

[a] Statistics for highest resolution shell are given in parentheses.